Figure 7. Impact of Frondoside A on the formation of capillary-like structures by HUVECs *in vitro.* A) Patterns of angiogenesis induced by human umbilical vein endothelial cells (HUVEC) cultured on Matrigel matrix in 96-well plates in the absence or presence of the Frondoside A. B) Quantification of tubular morphogenesis induced in HUVEC cells cultured in the absence or presence of Frondoside A. Tube formation was determined by the length of tube-like structures containing connected cells. Data are mean ± S.E.M. from three separate experiments. Asterisks indicate that significantly different values were obtained in the presence of the indicated inhibitors vs. the corresponding control stimulation. ***Significantly different at P<0.001. C) HUVEC cells were treated with vehicle (0.1% DMSO) and the indicated concentrations of Frondoside A. Viable cells were assayed as described in Materials and Methods. All experiments were repeated at least three times. *Columns*, mean; *bars*, S.E.M.
doi:10.1371/journal.pone.0053087.g007

Frondoside A also impairs lung cancer cell migration and invasion *in vitro* and metastasis *in vivo*

Cancer progression is associated with the abrogation of normal controls that limit cell migration and invasion, eventually leading to metastasis. Lung cancer patients are at high risk of recurrence in the form of metastatic disease. Metastasis starts with cell migration in the primary tumor, leading to local tissue invasion and entry into lymph or blood vessels. The ability of Frondoside A to reduce cellular migration was investigated using a classic *in vitro* wound healing model. Frondoside A reduced cellular migration of LNM35 cells in a concentration- and time-dependent manner (**Fig. 8A**). Similarly, Frondoside A impaired the invasion of LNM35 cells in matrigel invasion assay (**Fig. 8B**). Frondoside A

induced inhibition of cellular migration and matrigel invasion occurred without significant reduction of cell viability (**Fig. 1A**).

Next, we assessed the metastatic behavior of the human pulmonary cell line LNM35 by examining axillary lymph nodes. Histological examination of the lymph nodes in LNM35-bearing mice revealed the presence of LNM35 cells in all lymph nodes from both the control and Frondoside A treated mice (data not shown). In the control-treated group, the mean lymph nodes weight was 548.5+/−112.8 mg compared with 256+/−43.3 and 268.8+/−55.7 mg in the groups treated with Frondoside A 0.01 mg and 1 mg/kg/day, respectively (**Fig. 8C and 8D**).
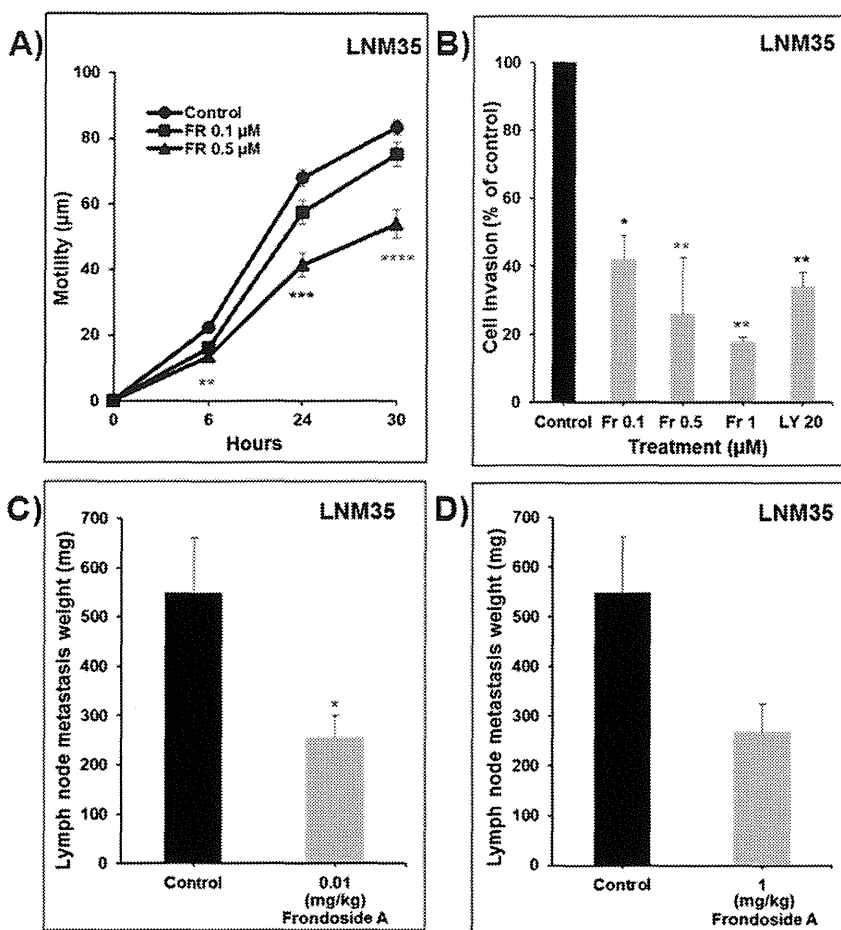
Figure 8. Frondoside A also impairs lung cancer cell migration and invasion *in vitro* **and metastasis** *in vivo.* A) Wounds were introduced in LNM35 confluent mono-layers cultured in the presence or absence (control) of Frondoside A (0.1–0.5 μM). The mean distance that cells travelled from the edge of the scraped area for 6, 24, and 30 h at 37°C was measured in a blinded fashion, using an inverted microscope (4× magnifications). Data are means ± S.E.M. of two independent experiments. B) LNM35 cells were incubated for 24 h in the presence or absence of Frondoside A (0.01–1 μM) and LY294002 (20 μM). Cells that invaded into Matrigel were scored as described in Materials and Methods. Columns, mean; bars, S.E.M. Lymph nodes metastasis weight of established human lung cancer xenografts treated with Frondoside A 0.01 mg/kg (C) and 1 mg/kg (D) every day for 25 days. Columns, mean; bars, S.E.M. *Significantly different at P<0.05, **Significantly different at P<0.01, ***Significantly different at P<0.001. doi:10.1371/journal.pone.0053087.g008

Frondoside A enhances the anticancer activity of cisplatin

As shown in **Fig. 9A**, daily administration of Frondoside A to nude mice reduced the growth of LNM35 human tumor xenografts by 40.3% at day 10. Inhibition of LNM35 tumor xenograft growth by Frondoside A was comparable with that produced by the DNA-damaging anticancer agent cisplatin (46.9%). Combined treatment of Frondoside A with cisplatin resulted in a remarkable potentiation (67.6%; *P<0.05*) of the cisplatin therapeutic effect (**Fig. 9A**). There were no manifest side effects of the combined treatment on animal behaviour or body weight (**Fig. 9B**).

Discussion

Despite advances in molecular biology of lung cancer, improved diagnosis, and even optimal target therapies, the current protocols for the treatment of lung cancer are still insufficient to produce striking clinical benefits and the cure of lung cancer patients remains unsuccessful. The current targeted therapy drugs develop resistance and they are very expensive and not available to the

majority of lung cancer patients in the world. Many drugs have relatively low activity; few patients are cured, with a brief, if any, increase in survival [17]. The history of anti-cancer agents, such as paclitaxel, shows that the mechanism of action was identified several years after its clinical efficacy was demonstrated. Despite not knowing the drug's mechanism of action, we believe that the *in vitro* as well as the strong *in vivo* anti-cancer effects of Frondoside A should translate in the clinic to a new potent anti- lung cancer agent.

In the present study, we investigated the impact of Frondoside A on lung cancer cells progression. We showed that Frondoside A caused concentration-responsive (0.01–5 μM) decreases in viability of LNM35, A549, and NCI-H460-Luc2 cells over 24 hours through the caspase 3/7-dependent cell death pathway. The IC50 concentrations (producing half-maximal inhibition) at 24 h were between 1.7 and 2.5 μM Frondoside A. These results are consistent with previously published results that low concentration of Frondoside A inhibits the growth of human pancreatic cancer cells and induced apoptosis through caspase 9/3/7, increased bax, decreased bcl-2 and mcl-1, and arrested cell cycle and up-regulated p21 [8], induced apoptosis in human leukemia cells via
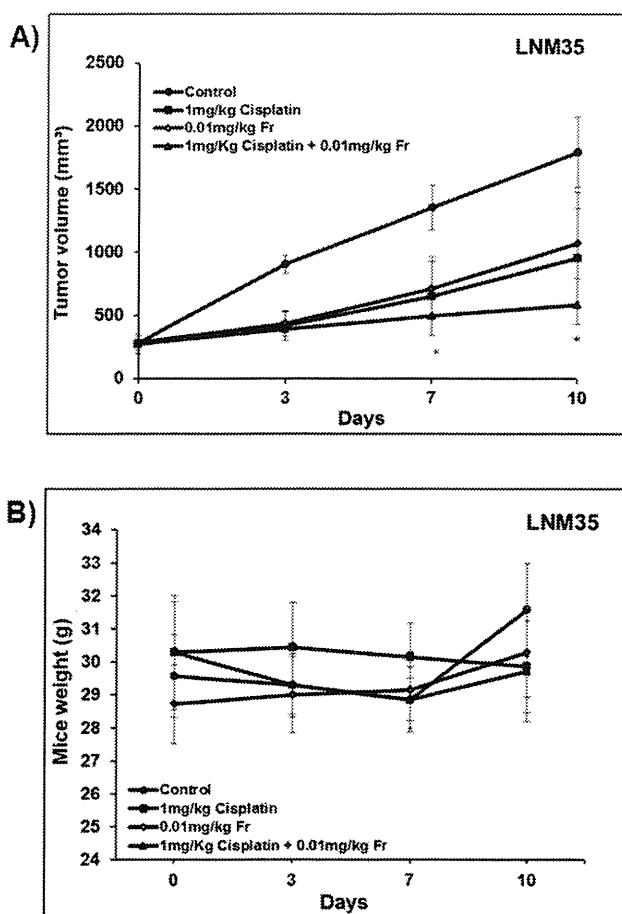
8

Figure 9. Antitumor activity of Frondoside A alone or in combination with the anticancer drug, cisplatin, against human lung tumor xenografts in athymic nude mice. A) Frondoside A enhances cisplatin efficacy against NSCLC LNM35 cells growing as xenografts. **B)** Impact of Frondoside A and cisplatin alone or in combination on body weight. *Significantly different at P<0.05.
doi:10.1371/journal.pone.0053087.g009

caspase activation [6], and significantly decreases the viability of the estrogen receptor (ER)-negative MDA-MB-231 breast cancer cells by inducing apoptosis via the Caspase9-Caspase3/7 intrinsic pathway [7]. It has also been demonstrated that Frondanol A5, an impure extract of *Cucumaria frondosa* skin from which Frondoside A is originally derived, induced growth inhibition at S and G2-M phase with a decrease in Cdc25c and an increase in p21$^{WAF1/CIP1}$ with significant apoptosis associated with H2AX phosphorylation and caspase-2 cleavage in the colon cancer-derived HCT116 cells [4]. A second paper also demonstrated that Frondanol-A5P, a polar precipitate sub-fraction of Frondanol-A5, inhibited proliferation and induced G2/M phase cell cycle arrest in two pancreatic cancer cells with decreased expression of cyclin A, cyclin B, and cdc25c [18]. This anticancer effect of Frondoside A is not tissue specific, and in this context we demonstrated that Frondoside A induced a concentration-dependent decrease in cell viability of the melanoma MDA-MB-435, the breast MCF-7, and the hepatoma HepG2 cells.

To assess the effects of Frondoside A on lung tumor development *in vivo*, LNM35 xenografts were made in immuno-

suppressed mice. We demonstrated that intraperitoneal administration of Frondoside A caused a strong regression of established tumors. Maximum inhibition was obtained with the low dose of 0.01 mg/kg/day for 25 days. A 100 times higher dose gives similar effects indicating that increasing the dose will not improve the anticancer efficacy of Frondoside A. The cancer inhibitory effect of Frondoside A has been observed previously on AsPC-1 pancreatic and MDA-MB-231 xenografts in athymic mice [7,8]. This antitumor effect of Frondoside A may be partly due to its immunostimulatory effect [13] and/or anti-angiogenic effect. In this study, we demonstrated for the first time, that Frondoside A is a strong anti-angiogenic agent. It reduces the microvessel density (measured by CD31 staining) in the xenografted tumor treated with Frondoside A and also significantly reverse basal and bFGF induced angiogenesis in the CAM angiogenesis assay. Similarly, Frondoside A completely suppressed capillary structure formation on Matrigel substratum by human endothelial cells.

Angiogenesis is an attractive target in cancer therapy not only because it supplies oxygen and nutrients for the survival of tumor cells but also provides the route for metastatic spread of these cancer cells. Cancer progression is associated with abrogation of the normal controls that limit cell migration and invasion, leading eventually to metastasis. As metastasis is the major cause of death in cancer patients, the development of new treatment regimens that reduce invasion and metastasis is highly important in cancer therapy. In this context, we demonstrated that Frondoside A induced a highly significant time- and concentration-dependent inhibition of cell migration, invasion *in vitro* and metastasis *in vivo*. These results are in agreement with our previous study showing that Frondoside A at concentrations that are not cytotoxic to the cells exerts a strong inhibitory effect on both the migratory and invasive properties of MDA-MB-231 breast cancer cells [7] and with another recent study demonstrating that Frondoside A inhibits breast cancer metastasis to the lungs [19].

Building on aforementioned results, and knowing from clinical trials that single agent treatments rarely result in clinical benefits to cancer patients, and that combination therapy are necessary for effective treatment of tumors, we investigated the therapeutic advantage of combination of cisplatin, (a first line treatment of lung cancer), with Frondoside A in nude mice bearing LNM35 xenografts. We found that Frondoside A enhances the inhibition of lung tumor growth induced by the chemotherapeutic agent cisplatin. These findings identify Frondoside A as a promising novel therapeutic agent for lung cancer and perhaps other cancers too.

Acknowledgments

Author Contributions

Conceived and designed the experiments: SA ODW. Performed the experiments: SA KA AG MAAS TEA. Analyzed the data: SA MB TEA ODW. Contributed reagents/materials/analysis tools: PC TT. Wrote the paper: SA ODW TEA MB TT.

- 177 -

References

1. Mann J (2002) Natural products in cancer chemotherapy: past, present and future. Nat Rev Cancer 2: 143–148.
2. Molinski TF, Dalisay DS, Lievens SL, Saludes JP (2009) Drug development from marine natural products. Nat Rev Drug Discov 8: 69–85.
3. Kuno T, Tsukamoto T, Hara A, Tanaka T (2012) Cancer chemoprevention through the induction of apoptosis by natural compounds. Journal of Biophysical Chemistry 3: 156–173.
4. Janakiram NB, Mohammed A, Zhang Y, Choi CI, Woodward C, et al. (2010) Chemopreventive effects of Frondanol A5, a Cucumaria frondosa extract, against rat colon carcinogenesis and inhibition of human colon cancer cell growth. Cancer Prev Res (Phila) 3: 82–91.
5. Girard M, Bélanger J, ApSimon JW, Garneau FX, Harvey C, et al. (1990) Frondoside A. A novel triterpene glycoside from the holothurians Cucumaria frondosa. Can J Chem 68: 11–18.
6. Jin JO, Shastina VV, Shin SW, Xu Q, Park JI, et al. (2009) Differential effects of triterpene glycosides, frondoside A and cucumarioside A2-2 isolated from sea cucumbers on caspase activation and apoptosis of human leukemia cells. FEBS Lett 583: 697–702.
7. Al Marzouqi N, Iratni R, Nemmar A, Arafat K, Ahmed Al Sultan M, et al. (2011) Frondoside A inhibits human breast cancer cell survival, migration, invasion and the growth of breast tumor xenografts. Eur J Pharmacol 668: 25–34.
8. Li X, Roginsky AB, Ding XZ, Woodward C, Collin P, et al. (2008) Review of the apoptosis pathways in pancreatic cancer and the anti-apoptotic effects of the novel sea cucumber compound, Frondoside A. Ann N Y Acad Sci 1138: 181–198.
9. Dempke WC, Suto T, Reck M (2010) Targeted therapies for non-small cell lung cancer. Lung Cancer 67: 257–274.
10. Spira A, Ettinger DS (2004) Multidisciplinary management of lung cancer. N Engl J Med 350: 379–392.
11. Korpanty G, Smyth E, Carney DN (2011) Update on anti-angiogenic therapy in non-small cell lung cancer: Are we making progress? J Thorac Dis 3: 19–29.
12. Kozaki K, Miyaishi O, Tsukamoto T, Tatematsu Y, Hida T, et al. (2000) Establishment and characterization of a human lung cancer cell line NCI-H460-LNM35 with consistent lymphogenous metastasis via both subcutaneous and orthotopic propagation. Cancer Res 60: 2535–2540.
13. Aminin DL, Agafonova IG, Kalinin VI, Silchenko AS, Avilov SA, et al. (2008) Immunomodulatory properties of frondoside A, a major triterpene glycoside from the North Atlantic commercially harvested sea cucumber Cucumaria frondosa. J Med Food 11: 443–453.
14. Aminin DL, Koy C, Dmitrenok PS, Müller-Hilke B, Koczan D, et al. (2009) Immunomodulatory effects of holothurian triterpene glycosides on mammalian splenocytes determined by mass spectrometric proteome analysis. J Proteomics 72: 886–906.
15. Derycke L, Morbidelli L, Ziche M, De Wever O, Bracke M, et al. (2006) Soluble N-cadherin fragment promotes angiogenesis. Clin Exp Metastasis 23: 187–201.
16. Harris-Hooker SA, Gajdusek CM, Wight TN, Schwartz SM (1983) Neovascular responses induced by cultured aortic endothelial cells. J Cell Physiol 114: 302–310.
17. Hait WN (2010) Anticancer drug development: the grand challenges. Nat Rev Drug Discov 9: 253–254.
18. Roginsky AB, Ding XZ, Woodward C, Ujiki MB, Singh B, et al. (2010) Anti-pancreatic cancer effects of a polar extract from the edible sea cucumber, Cucumaria frondosa. Pancreas 39: 646–652.
19. Ma X, Kundu N, Collin PD, Goloubeva O, Fulton AM (2011) Frondoside A inhibits breast cancer metastasis and antagonizes prostaglandin E receptors EP4 and EP2. Breast Cancer Res Treat.

- 178 -

Conversion from the "oncogene addiction" to "drug addiction" by intensive inhibition of the EGFR and MET in lung cancer with activating *EGFR* mutation

Kenichi Suda [a,c], Kenji Tomizawa [a], Hirotaka Osada [b], Yoshihiko Maehara [c], Yasushi Yatabe [d], Yoshitaka Sekido [b], Tetsuya Mitsudomi [a,*]

[a] Department of Thoracic Surgery, Aichi Cancer Center Hospital, 1-1 Kanokoden, Chikusa-ku, Nagoya, Japan
[b] Division of Molecular Oncology, Aichi Cancer Center Research Institute, 1-1 Kanokoden, Chikusa-ku, Nagoya, Japan
[c] Department of Surgery and Science, Graduate School of Medical Science, Kyushu University, 3-1-1 Maidashi, Higashi-ku, Fukuoka, Japan
[d] Department of Pathology and Molecular Diagnostics, Aichi Cancer Center Hospital, 1-1 Kanokoden, Chikusa-ku, Nagoya, Japan

ARTICLE INFO

ABSTRACT

Emergence of acquired resistance is virtually inevitable in patients with a mutation in the epidermal growth factor receptor gene (*EGFR*) treated with EGFR tyrosine kinase inhibitors (TKIs). Several novel TKIs that may prevent or overcome the resistance mechanisms are now under clinical development. However, it is unknown how tumor cells will respond to intensive treatment using these novel TKIs. We previously established HCC827EPR cells, which are T790M positive, through combined treatment with erlotinib and a MET-TKI from erlotinib-hypersensitive HCC827 cells. In this study, we treated HCC827EPR cells sequentially with an irreversible EGFR-TKI, CL-387,785, to establish resistant cells (HCC827CLR), and we analyzed the mechanisms responsible for resistance. In HCC827CLR cells, *PTEN* expression was downregulated and Akt phosphorylation persisted in the presence of CL-387,785. Akt inhibition restored CL-387,785 sensitivity. In addition, withdrawal of CL-387,785 reduced cell viability in HCC827CLR cells, indicating that these cells were "addicted" to CL-387,785. HCC827CLR cells overexpressed the EGFR, and inhibition of the EGFR or MEK–ERK was needed to maintain cell proliferation. Increased senescence was observed in HCC827CLR cells in the drug-free condition. Through long-term culture of HCC827CLR cells without CL-387,785, we established HCC827-CL-387,785-independent cells, which exhibited decreased *EGFR* expression and a mesenchymal phenotype. In conclusion, *PTEN* downregulation is a newly identified mechanism underlying the acquired resistance to irreversible EGFR-TKIs after acquisition of T790M against erlotinib. This series of experiments highlights the flexibility of cancer cells that have adapted to environmental stresses induced by intensive treatment with TKIs.

© 2011 Elsevier Ireland Ltd. All rights reserved.

1. Introduction

Epidermal growth factor receptor (EGFR)-mutated lung cancers are addicted to mutated EGFR. Patients with lung cancers harboring *EGFR* mutations often dramatically respond to orally available EGFR tyrosine kinase inhibitors (TKIs) [1–3]. However, acquired resistance develops in almost all patients, usually within 1 year, and this limits the improvement in patient outcomes. Therefore, it is essential to develop treatment strategies that can prevent or overcome the emergence of acquired resistance.

The common mechanisms underlying acquired resistance include the T790M *EGFR* secondary mutation and *MET* gene amplification, which are present in about 50% and 5–20% of the tumors with acquired resistance, respectively [4–7]. Because the T790M

mutation confers resistance by increasing the affinity of the EGFR for ATP relative to that for TKIs [8], several kinds of irreversible TKIs that covalently bind to cysteine 797 at the catalytic pocket of EGFR are expected to overcome this type of resistance. In addition, several MET-TKIs are also now under clinical development. Intensive treatment using these kinase inhibitors may be applied to clinic in the near future, but at present, it is unknown how tumor cells will respond to such treatment.

HCC827 lung adenocarcinoma cells harbor a deletion mutation in exon 19 of *EGFR* and are very sensitive to EGFR-TKIs. A recent report has revealed the preexistence of minor clones with *MET* amplification (about 0.1%) in HCC827 cells untreated with EGFR-TKIs [9], and this cell line often acquires resistance to EGFR-TKIs through *MET* amplification [6,9,10]. Therefore, we treated HCC827 cells with increasing concentrations of erlotinib in the presence of the MET-TKI, PHA-665,752, and obtained cells resistant to the combination of both drugs; we have designated these HCC827EPR cells. HCC827EPR cells have an acquired EGFR T790M mutation

* Corresponding author. Tel.: +81 52 762 6111; fax: +81 52 764 2963.
 E-mail address: mitsudom@aichi-cc.jp (T. Mitsudomi).

and are sensitive to the irreversible EGFR-TKI, CL-387,785. We decided to establish an *in vitro* model of acquired resistance to CL-387,785 sequentially from HCC827EPR cells with T790M mutation, and investigated the mechanisms responsible for the resistance.

2. Materials and methods

2.1. Cell lines and reagents

The *EGFR* mutant human lung adenocarcinoma cell line HCC827 (del L746_A750) was a kind gift of Dr. Adi F. Gazdar. A subclone of HCC827EPR cells (HCC827EPR.S10 cells) was developed previously in our laboratory [10]. HCC827EPR.S10 cells harbor the T790M mutation in addition to the exon 19 deletion mutation in the *EGFR* gene. These cells were cultured in RPMI-1640 medium supplemented with 5% FBS and 1× antibiotic–antimycotic solution (Invitrogen, Carlsbad, CA) at 37 °C in a humidified incubator with 5% CO_2.

Erlotinib was kindly provided by Hoffmann-La Roche Inc. (Nutley, NJ). CL-387,785 was purchased from Calbiochem (San Diego, CA). PHA-665,752 was purchased from Tocris Bioscience (Ellisville, MO). Two kinds of MEK inhibitor (PD0325901 and AZD6244) and an AKT 1/2 Kinase Inhibitor were purchased from Wako (Osaka, Japan).

2.2. Generation of in vitro CL-387,785-resistant cells

CL-387,785-resistant HCC827 (HCC827CLR) cells were developed from HCC827EPR.S10 cells through the chronic, repeated exposure to increasing concentrations of CL-387,785 from 100 nM to 1 μM, as described previously [6]. CL-387,785-free HCC827 (HCC827CLF) cells were developed from HCC827CLR cells by culturing cells without any drugs for 1 month.

Cell proliferation was measured using TetraColor ONE (Seikagaku-kogyo, Tokyo, Japan), according to the manufacturer's instructions [10]. Parental or resistant cells were incubated for 24 h and then an additional 72 h with drug(s) at the concentrations indicated, and cell growth was assessed.

2.3. Mutation, gene copy number, and expression analyses

Genomic DNA was extracted using a FastPure DNA Kit (Takara Bio, Otsu, Japan). Total RNA was prepared using a mirVana miRNA Isolation Kit (Qiagen, Valencia, CA). Random-primed, first-strand cDNA was synthesized from total RNA using Superscript II (Invitrogen), according to the manufacturer's instructions.

Mutation analysis of exons 18–21 of the *EGFR* gene was performed via direct sequencing after one-step reverse transcription PCR (RT-PCR) from total RNA using the Qiagen OneStep Reverse Transcription PCR Kit (Qiagen), as reported previously [11].

The numbers of copies of the *MET* gene and the *EGFR* gene relative to a *LINE-1* repetitive element were measured using quantitative real-time PCR using the SYBR Green Method (Power SYBR Green PCR Master Mix; Qiagen) on an ABI PRISM 7900HT Sequence Detection System (Applied Biosystems, Foster City, CA) as described previously [6,12]. Normal genomic DNA was used as a standard sample.

Quantitative real-time RT-PCR was performed on first-strand cDNA using TaqMan probes and the TaqMan Universal PCR Master Mix (Applied Biosystems). TaqMan probes for *EGFR* and *PTEN* were purchased from Applied Biosystems and the amplification was performed on an ABI PRISM 7900HT Sequence Detection System (Applied Biosystems). Quantification was performed in triplicate and the level of expression of 18S rRNA was used as an internal control.

2.4. Phospho-RTK array and Western blot analysis

A Human Phospho-RTK Array Kit (R&D Systems, Minneapolis, MN) was used to measure the relative level of tyrosine phosphorylation of 42 distinct receptor tyrosine kinases (RTKs), according to the manufacturer's instructions as described previously [10].

The preparation of total cell lysates and immunoblotting was performed as described previously. Briefly, cells were cultured until subconfluent, and the medium was changed to 5% FBS containing dimethyl sulfoxide (DMSO) or the indicated concentration of the drug(s) for the durations indicated. Cells were rinsed in PBS, lysed in SDS sample buffer, and homogenized. The total cell lysate (30 μg) was subjected to SDS PAGE and transferred to Immobilon-P polyvinylidene difluoride membranes (Millipore, Bedford, MA). After blocking with 5% nonfat dry milk, the membranes were incubated with primary antibodies, washed with PBS, reacted with secondary antibodies, treated with ECL solution, and exposed to film. All antibodies were purchased from Cell Signaling Technology (Beverly, MA).

2.5. Senescence-associated β-galactosidase (SA-β-gal assay)

SA-β-gal activity was measured using an SA-β-gal staining kit purchased from BioVision Research Products (Mountain View, CA), according to the manufacturer's instructions. Senescent cells were identified as blue-stained cells by standard light microscopy.

3. Results

3.1. Establishment of in vitro CL-387,785-resistant cells

First, we analyzed the growth-inhibitory effects of CL-387,785 in HCC827 cells and in HCC827EPR.S10 cells (abbreviated as HCC827EPR cells), and we identified that both cell lines are sensitive to this drug (IC_{50}; <10 nM in HCC827 cells and 380 nM in HCC827EPR cells, Fig. 1A).

We then generated CL-387,785-resistant cells from HCC827EPR cells by growing the cells in increasing concentrations of CL-387,785 (from 100 nM to a final concentration of 1 μM) for up to 3 months *in vitro*, as described previously [9,10]. The resultant CL-387,785-resistant cells (designated HCC827CLR cells) were maintained in the presence of 1 μM CL-387,785.

We extracted RNA and genomic DNA from HCC827CLR cells and analyzed the mutations, amplification, and gene expression of the candidate genes. Mutation analyses revealed that HCC827CLR cells harbored the T790M mutation in a similar ratio of mutant versus wild-type alleles to that of HCC827EPR cells (Fig. 1B). In addition, the *EGFR* gene copy number in HCC827CLR cells, assessed using quantitative real-time PCR, was identical to that observed in HCC827 cells and in HCC827EPR cells (25.0, 24.8, and 26.0 times compared with normal genomic DNA). Because HCC827 cells and their descendants do not have wild-type *EGFR* allele, these results indicate that the copy number of T790M containing allele in HCC827CLR cells is identical to that in HCC827EPR cells. On the other hand, the *MET* gene copy number in HCC827CLR cells was also identical to that observed in HCC827 cells and in HCC827EPR cells (1.3, 1.5, and 1.9 times compared with normal genomic DNA). In addition, the MET-TKI PHA-665,752 did not restore CL-387,785 sensitivity in HCC827CLR cells (data not shown). We and others have shown recently that the epithelial to mesenchymal transition (EMT) is involved in the acquired resistance to EGFR-TKIs [13–15]. However, HCC827CLR cells showed strong E-cadherin and weak vimentin expression (Fig. 1C, right lane) in addition to a tightly
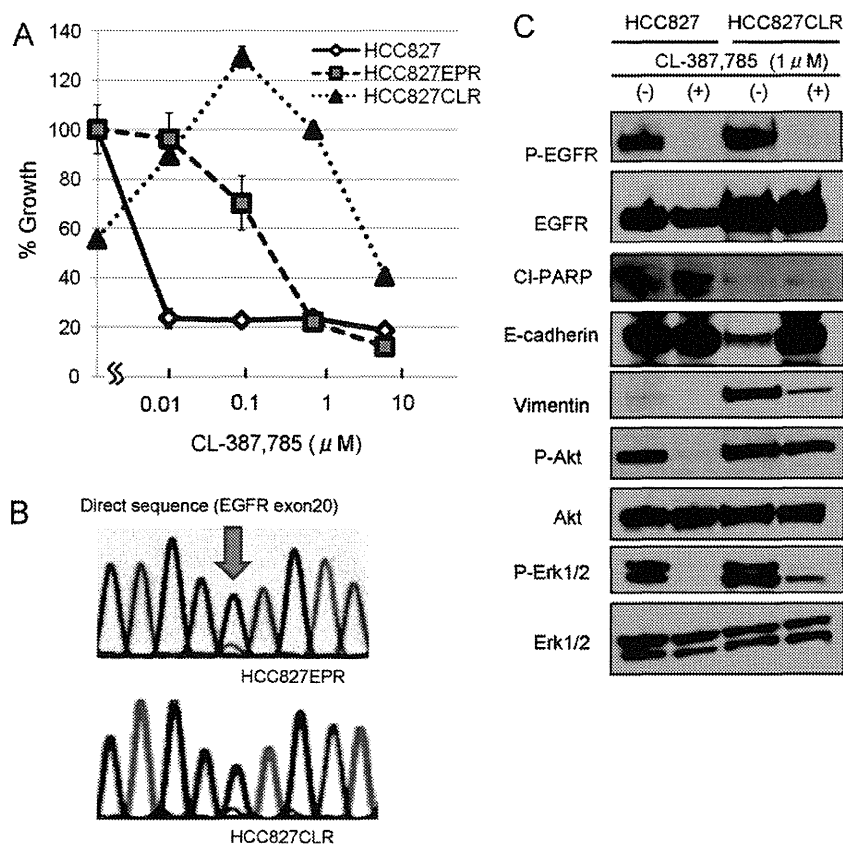
Fig. 1. Analysis of EGFR and candidate intracellular molecules in HCC827CLR cells. (A) Growth-inhibitory effect of CL-387,785. Percentage growth was calculated relative to DMSO-treated controls in HCC827 or HCC827EPR cells, and relative to 1 μM CL-387,785 (maintenance concentration) treated cells in HCC827CLR cells. (B) HCC827EPR and HCC827CLR cells harbored the T790M mutation in a similar mutant/wild-type allele ratio. Antisense strands of sequencing chromatograms for EGFR mRNA are shown. Blue arrow, C to T substitution at nucleotide 2369 (G to A on the antisense strand), which results in the T790M mutation. (C) Increased EGFR expression and maintained Akt phosphorylation in HCC827CLR cells. Western blotting was used to analyze HCC827 cells incubated for 24 h with DMSO or 1 μM CL-387,785, and HCC827CLR cells without CL-387,785 for two passages or those with continuous exposure to 1 μM CL-387,785. (For interpretation of the references to color in this figure legend, the reader is referred to the web version of this article.)

conjunct epithelial cell-like appearance (Fig. 2A), indicating that the acquired resistance in HCC827CLR cells was unrelated to the EMT.

3.2. PTEN downregulation and restoration of CL-387,785 sensitivity by Akt inhibition in HCC827CLR cells

In the analysis of downstream molecules of EGFR, we identified sustained phosphorylation of Akt in HCC827CLR cells in the presence of CL-387,785, although phosphorylation of ERK1/2 was inhibited effectively (Fig. 1C). First, we examined the relative expression of PTEN in these cells because PTEN downregulation and increased Akt phosphorylation have been reported to cause gefitinib resistance in PC9 cells [16]. As expected, HCC827CLR cells showed significant downregulation of PTEN expression, although that of HCC827EPR cells was similar to that of HCC827 cells (Fig. 3A). Therefore, we treated these cells with the Akt inhibitor, AKT 1/2 Kinase Inhibitor. The growth-inhibitory effect of AKT 1/2 Kinase Inhibitor alone was mild in HCC827, HCC827EPR, and HCC827CLR cells (Fig. 3B).

Next, we treated HCC827CLR cells with CL-387,785 combined with 1 μM AKT 1/2 Kinase Inhibitor. AKT 1/2 Kinase Inhibitor effectively suppressed Akt phosphorylation and increased cleaved PARP expression (Fig. 3C), and Akt inhibition restored CL-387,785 sensitivity (IC_{50}: 173 nM, Fig. 3D).

3.3. "Drug addiction" and increased expression of the EGFR in HCC827CLR cells

Further observation identified greater proliferation of HCC827CLR cells with 1 μM of CL-387,785 than with DMSO alone (the concentration of DMSO was the same in both experimental conditions; Fig. 1A). We also found marked morphological differences in HCC827CLR cells between those treated with (Fig. 2A) and without (Fig. 2B and C) CL-387,785. The morphological features observed in the cells without CL-387,785 included spindle-shaped cells, loss of intercellular connections, and increased formation of pseudopodia, suggesting the involvement of the EMT, and enlarged cells and flattened cell morphology within 1 week of drug withdrawal (Fig. 2C), suggesting the involvement of premature senescence.

We first used immunoblot analysis to analyze the protein expression of the EMT markers, EGFR, and its downstream molecules (Fig. 1C). Total EGFR expression was significantly higher in HCC827CLR cells, although CL-387,785 effectively suppressed the phosphorylation of EGFR in HCC827 and HCC827CLR cells. We also confirmed the significantly higher EGFR mRNA expression in HCC827CLR cells compared with HCC827 and HCC827EPR cells (Fig. 4A). However, EGFR gene copy number was identical in HCC827CLR, HCC827, and HCC827EPR cells as described above. Expression of cleaved PARP, one marker of apoptosis, was observed in HCC827 cells treated with CL-387,785 but not in HCC827CLR
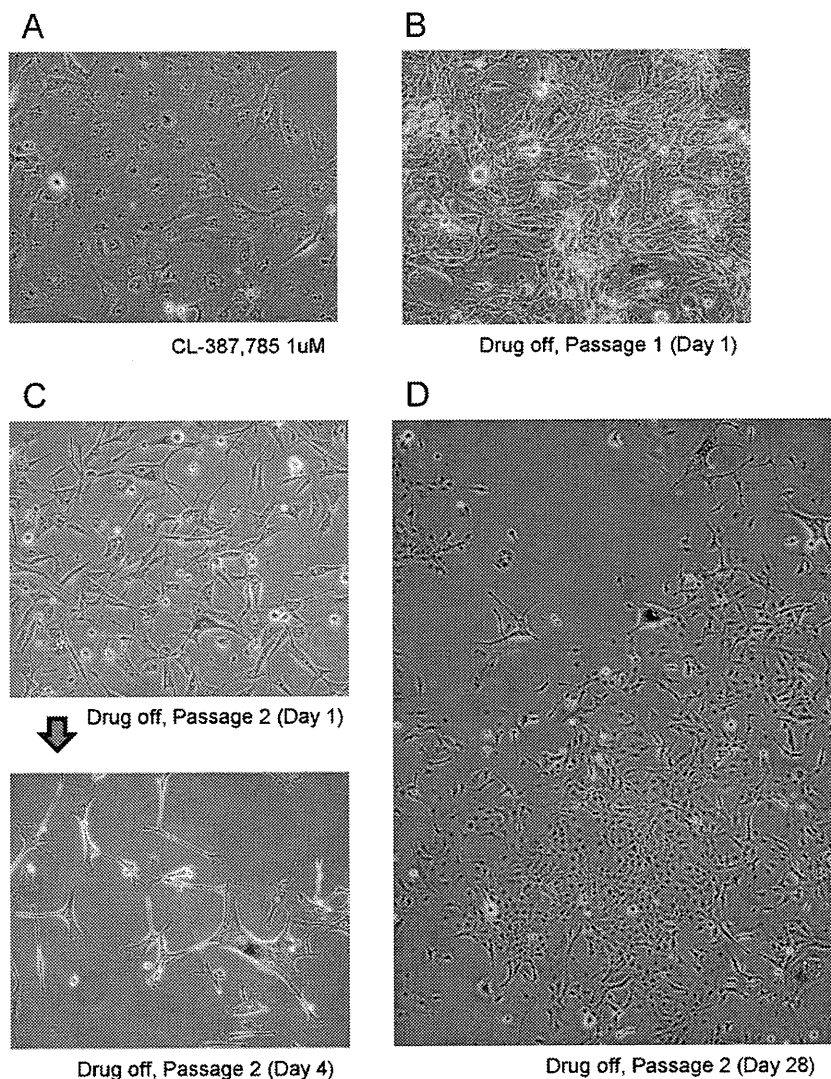
A

CL-387,785 1uM

B

Drug off, Passage 1 (Day 1)

C

Drug off, Passage 2 (Day 1)

Drug off, Passage 2 (Day 4)

D

Drug off, Passage 2 (Day 28)

Fig. 2. Morphological differences between HCC827CLR cells treated with CL-387,785 (A), those not treated with CL-387,785 (B and C), and HCC827CLF cells (D) observed under standard light microscopy. Senescence-associated β-galactosidase is stained blue.

cells treated with or without CL-387,785 (Fig. 1C). HCC827CLR cells without CL-387,785 showed significantly increased expression of vimentin and downregulation of E-cadherin (Fig. 1C), which were consistent with their morphological changes.

3.4. Need for MEK inhibition for the maintenance of cell proliferation

Because Akt inhibition could not restore proliferation of HCC827CLR cells in the absence of CL-387,785 (Fig. 3A), we next analyzed the inhibitory effects of MEK–ERK pathway, the other main downstream signaling from the EGFR, using a MEK inhibitor PD0325901. Both HCC827 parental cells and HCC827EPR cells showed moderate sensitivity to this drug (Fig. 4C, left). Interestingly, PD0325901 restored the epithelial morphology in HCC827CLR cells without CL-387,785 treatment and restored cell proliferation in HCC827CLR cells without CL-387,785 (Fig. 4C, left). We performed the same experiments using another MEK inhibitor, ADZ6244, and obtained the same results (Fig. 4C, right). Western blot analysis showed that PD0325901 suppressed the phosphorylation of ERK1/2 more effectively than did AZD6244 (Fig. 4B); this result is consistent with the finding that PD0325901 has a greater "proliferation recovery effect" than does AZD6244.

3.5. Senescence reaction in HCC827CLR cells without EGFR inhibition

The growth-inhibitory effect of HCC827CLR cells caused by CL-387,785 withdrawal could not be explained by apoptosis (Fig. 1C). We next stained for SA-β gal in HCC827CLR cells with or without CL-387,785 because the following results suggested the involvement of oncogene-induced senescence: (i) the morphological changes described above were consistent with senescence, (ii) EGFR or ERK inhibition restored proliferation in HCC827CLR cells, and (iii) hyperactivation of the RAS–MEK–ERK pathway has been reported to cause oncogene induced senescence [17]. Few HCC827CLR cells treated with CL-387,785 (1.0%) were positive for SA-β gal (Fig. 2A), but many more HCC827CLR cells without CL-387,785 (9.4%) were positive for SA-β gal (Fig. 2B and C). These findings indicate that oncogene-induced senescence is one cause of this "drug addiction".

3.6. Establishment of HCC827CLF cells

As shown in Fig. 2C, many HCC827CLR cells died when they were maintained without CL-387,785. We cultured these cells (passage 2 after CL-387,785 withdrawal) without any passage until
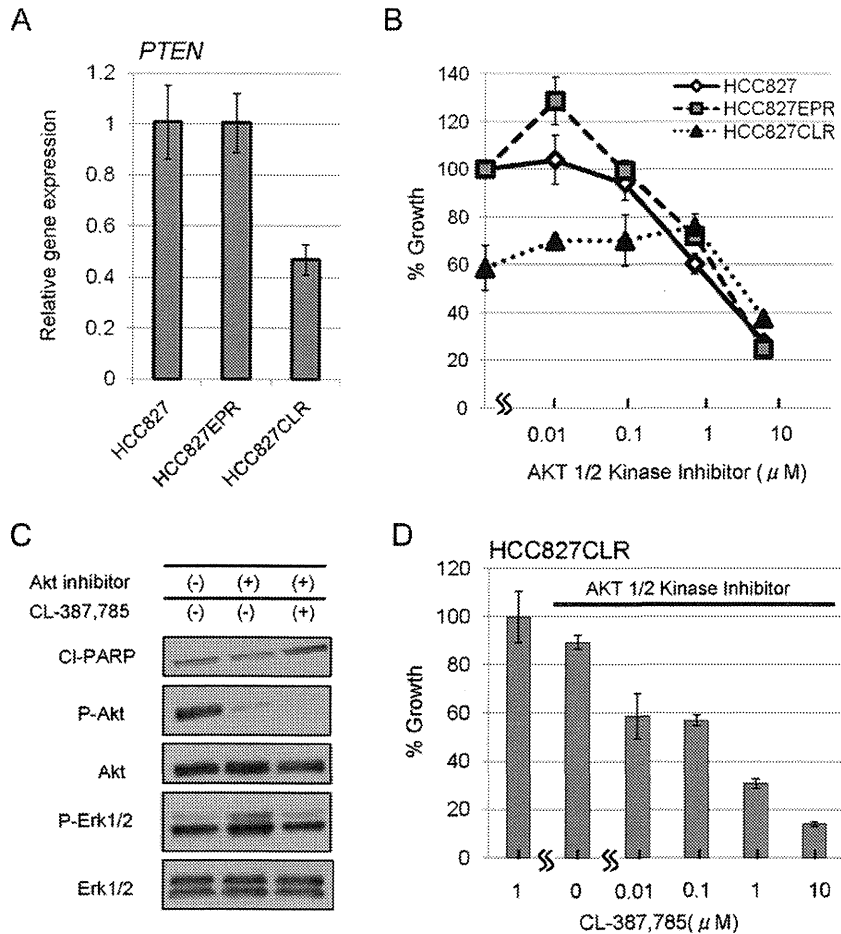
Fig. 3. Combined effect of AKT 1/2 Kinase Inhibitor and CL-387,785 in HCC827CLR cells. (A) Quantitative real-time RT-PCR identified HCC827CLR cells showed downregulation of *PTEN* expression. (B) Growth-inhibitory effect of Akt inhibitor monotherapy. Percentage growth was calculated relative to DMSO-treated controls in HCC827 or HCC827EPR cells, and relative to 1 μM CL-387,785-treated cells in HCC827CLR cells. (C) HCC827CLR cells were cultured for two passages without CL-387,785 and then incubated for 48 h with DMSO, 1 μM AKT 1/2 Kinase Inhibitor, or the combination of AKT 1/2 Kinase Inhibitor and 1 μM CL-387,785, and then analyzed by Western blotting. (D) HCC827CLR cells were sensitive to CL-387,785 in the presence of an Akt inhibitor. Percentage growth was calculated relative to 1 μM CL-387,785-treated cells.

the cells began to proliferate again. After 4 weeks, some colonies were observed, and these cells were designated HCC827CLF (CL-387,785-free) cells (Fig. 2D). In the mutational analysis, HCC827CLF cells harbored the T790M mutation in a similar ratio of mutant versus wild-type alleles compared with HCC827EPR cells and HCC827CLR cells (data not shown). HCC827CLF cells were negative for SA-β gal and could be maintained without CL-387,785. HCC827CLF cells preserved the mesenchymal phenotype (e.g., spindle-shaped morphology, expression of vimentin, and loss of E-cadherin, Fig. 5A), irrespective of the presence of CL-387,785. *EGFR* expression decreased to the same level as that observed in HCC827EPR cells in translational (Fig. 4A) and in transcriptional (Fig. 5A) levels. HCC827CLF cells were mildly resistant to CL-387,785; about 60% of cells survived in the presence of 1 μM CL-387,785 (Fig. 5B).

4. Discussion

The second-generation EGFR-TKIs that can irreversibly and covalently bind to cysteine 797 of the EGFR are expected to overcome the acquired resistance conferred by the T790M mutation [18]. The EGFR-TKIs that belong to this class (e.g., PF299804 and BIBW2992) are currently under clinical evaluation [18] and these drugs may be administered to some patients who acquire the T790M mutation. However, little is known about how cancer cells behave in this situation.

Ercan et al. generated PF299804-resistant cell lines from gefitinib-resistant PC9 cells (*EGFR* delE746_A750 with T790M) and found that amplification of *EGFR* T790M was the cause of the resistance [19]. In the present study, although our CL-387,785-resistant cells (HCC827CLR cells) did not harbor the T790M amplification (Fig. 1B), *PTEN* expression was downregulated and Akt phosphorylation was sustained in the presence of CL-387,785 (Fig. 1C). We also observed that Akt inhibition restored the sensitivity to CL-387,785 in HCC827CLR cells (Fig. 3D). Downregulation of *PTEN* has been reported to cause primary erlotinib resistance in *EGFR* mutant lung cancer cells [20], and to cause acquired resistance to gefitinib in PC9 cells [16]. We found that acquired resistance caused by *PTEN* downregulation occurred in an *EGFR*-mutant lung cancer cell line other than PC9 cells. We also found that *PTEN* downregulation was the mechanism responsible for "secondary" acquired resistance to EGFR-TKIs after the acquisition of the T790M mutation. Our results suggest that the combined inhibition of the PI3K–Akt pathway along with EGFR inhibition may be necessary in the treatment of *EGFR*-mutant lung cancers.

The other finding in this study was the "drug addiction" phenomenon in HCC827CLR cells. In other words, HCC827CLR cells were not only able to proliferate in the presence of CL-387,785, but also underwent senescence, as evidenced by the increased expression of SA-β gal upon withdrawal of CL-387,785. HCC827CLR cells showed increased *EGFR* expression. The senescence-inhibitory activity of CL-387,785 could be substituted by erlotinib. We also
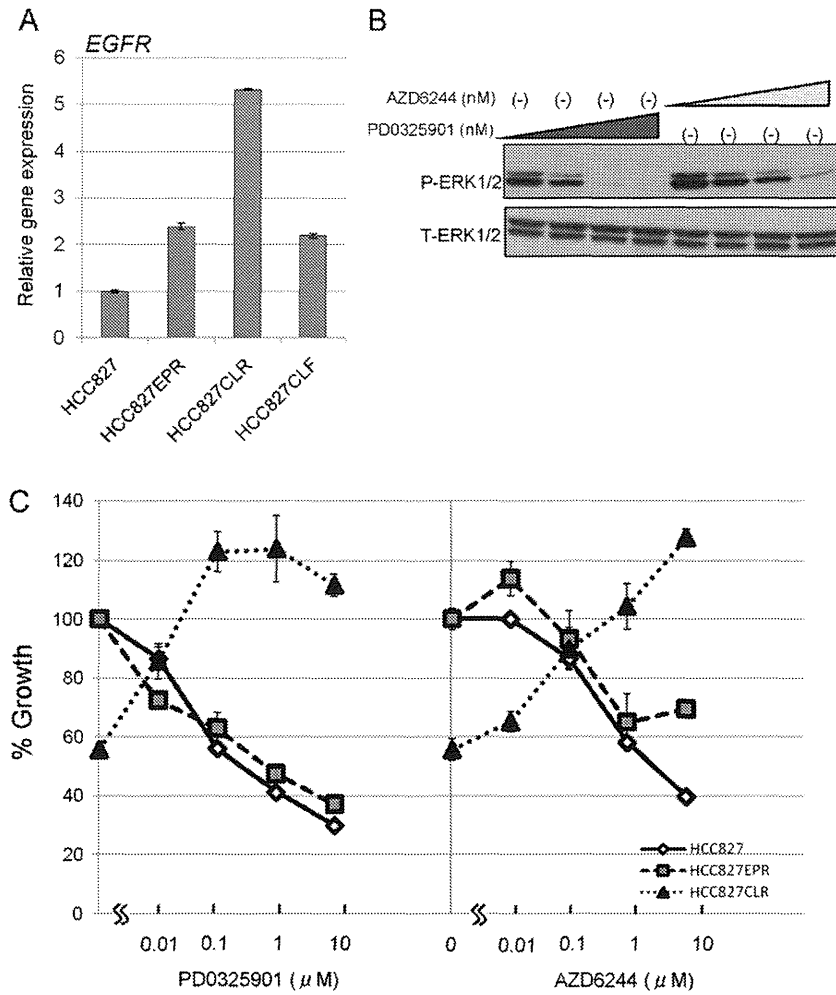
Fig. 4. Restoration of proliferation by MEK inhibitors in HCC827CLR cells not treated with CL-387,785. (A) *EGFR* gene expression increased in HCC827CLR cells. Relative gene expressions compared with HCC827 parental cells were analyzed by quantitative real-time RT-PCR. (B) HCC827CLR cells were cultured for two passages without CL-387,785 and then incubated for 48 h with the indicated concentrations (10 nM, 100 nM, 1000 nM, or 10000 nM) of PD0325901 or AZD6244, and examined by Western blotting. (C) Growth-inhibitory effect of MEK inhibitor monotherapy. Percentage growth was calculated relative to DMSO-treated controls in HCC827 or HCC827EPR cells, and relative to 1 μM CL-387,785-treated cells in HCC827CLR cells.
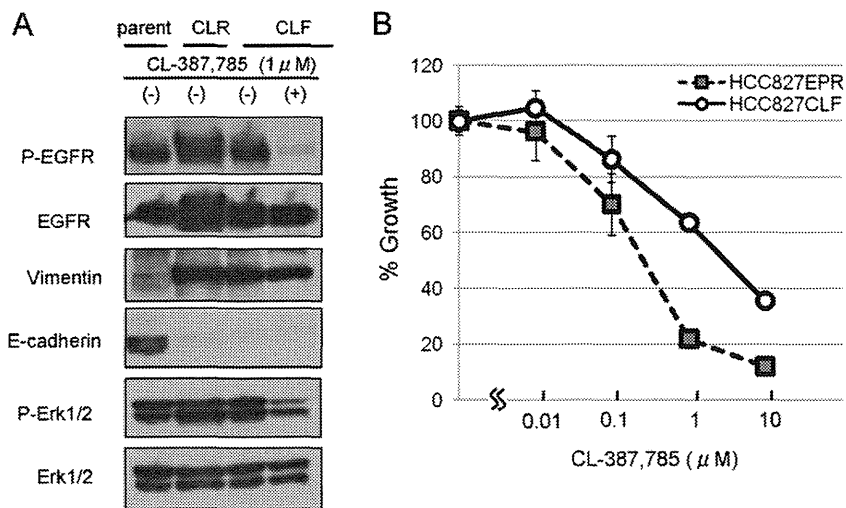

Fig. 5. Analysis of HCC827CLF cells. (A) HCC827CLF cells were incubated for 48 h with DMSO or 1 μM CL-387,785 and examined by Western blotting. (B) Growth-inhibitory effect of CL-387,785 in HCC827CLF cells. Percentage growth was calculated relative to DMSO-treated controls. The results for HCC827EPR cells (data from Fig. 1A) are shown for comparison.
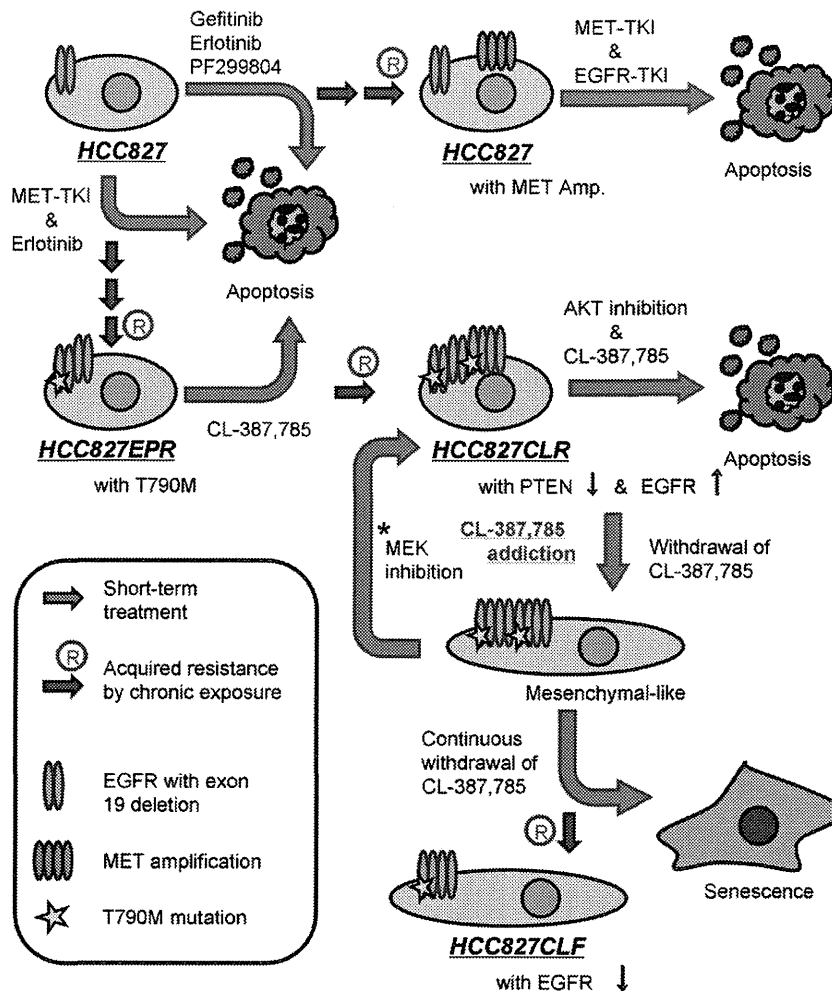
Fig. 6. Schema of the phenotypic changes in HCC827 lung cancer cells from "oncogene addiction" to "acquired resistance" and further to "drug addiction" during adaptation to intensive EGFR and MET kinase inhibition. HCC827CLR cells were addicted to CL-387,785 and withdrawal of CL-387,785 caused mesenchymal-like phenotype, and further, increased senescence. However, MEK inhibition restored cell proliferation in HCC827CLR cells without CL-387,785 (*).

found that MEK–ERK inhibition but not Akt inhibition could restore this activity. Because the KRAS–MEK–ERK pathway is reported to be related to senescence [17,21,22], we suggest that the mechanism responsible for this "drug addiction" is senescence by a hyperactivated EGFR–MEK–ERK pathway conferred by the sudden dysregulation of overexpressed *EGFR* upon withdrawal of CL-387,785. This is consistent with the result showing that EGFR expression in HCC827CLR cells returned to the same level as in the original HCC827EPR cells (Fig. 4A) and resumed to grow after a month of culture without the drug (HCC827CLF cells).

Fig. 6 illustrates how the HCC827 lung cancer cells behaved after intensive and sequential treatment with several TKIs. HCC827 cells had the potential to develop *MET* amplification, the T790M mutation, *EGFR* overexpression, *PTEN* downregulation, and the EMT so that they could adapt and survive in an environment with potent and selective TKI treatment. Although the overexpressed *EGFR* seemed to be a vulnerability in the absence of EGFR-TKIs, perhaps through oncogene-induced senescence, *EGFR* expression could decrease readily in HCC827CLR cells cultured in the drug-free condition.

This condition we call "drug addiction" contrasts with the so-called "flare effect" after withdrawal of EGFR-TKIs after the patient experiences progressive disease. Riely et al. analyzed ten patients with acquired resistance to EGFR-TKI and observed a median 18% increase in the SUVmax (standard uptake value) in positron emission tomography and 9% increase in tumor diameter, 3 weeks after

stopping the EGFR-TKI [23]. However, we believe that, in some situations after intensive treatment with EGFR inhibitors, the opposite may occur as shown in our *in vitro* study.

In conclusion, we observed *PTEN* downregulation as an acquired resistance mechanism in HCC827CLR cells established through intensive and sequential TKI treatment. Our series of experiments highlights the flexibility of cancer cells that have adapted to environmental stresses induced by intensive and sequential treatment with potent and selective TKIs. Cancer cells sometimes become not only resistant to the TKI but also dependent on or addicted to the TKI. This highly flexible and plastic nature of the cancer cells should be considered when trying to improve the outcomes in patients with lung cancer.

Conflict of interest

Acknowledgments

References

[1] Mok TS, Wu YL, Thongprasert S, Yang CH, Chu DT, Saijo N, et al. Gefitinib or carboplatin–paclitaxel in pulmonary adenocarcinoma. N Engl J Med 2009;361:947–57.

[2] Mitsudomi T, Morita S, Yatabe Y, Negoro S, Okamoto I, Tsurutani J, et al. Gefitinib versus cisplatin plus docetaxel in patients with non-small-cell lung cancer harbouring mutations of the epidermal growth factor receptor (WJTOG3405): an open label, randomised phase 3 trial. Lancet Oncol 2010;11:121–8.

[3] Maemondo M, Inoue A, Kobayashi K, Sugawara S, Oizumi S, Isobe H, et al. Gefitinib or chemotherapy for non-small-cell lung cancer with mutated EGFR. N Engl J Med 2010;362:2380–8.

[4] Pao W, Miller VA, Politi KA, Riely GJ, Somwar R, Zakowski MF, et al. Acquired resistance of lung adenocarcinomas to gefitinib or erlotinib is associated with a second mutation in the EGFR kinase domain. PLoS Med 2005;2:e73.

[5] Kobayashi S, Boggon TJ, Dayaram T, Janne PA, Kocher O, Meyerson M, et al. EGFR mutation and resistance of non-small-cell lung cancer to gefitinib. N Engl J Med 2005;352:786–92.

[6] Engelman JA, Zejnullahu K, Mitsudomi T, Song Y, Hyland C, Park JO, et al. MET amplification leads to gefitinib resistance in lung cancer by activating ERBB3 signaling. Science 2007;316:1039–43.

[7] Sequist LV, Waltman BA, Dias-Santagata D, Digumarthy S, Turke AB, Fidias P, et al. Genotypic and histological evolution of lung cancers acquiring resistance to EGFR inhibitors. Sci Transl Med 2011;3, 75ra26.

[8] Yun CH, Mengwasser KE, Toms AV, Woo MS, Greulich H, Wong KK, et al. The T790M mutation in EGFR kinase causes drug resistance by increasing the affinity for ATP. Proc Natl Acad Sci USA 2008;105:2070–5.

[9] Turke AB, Zejnullahu K, Wu YL, Song Y, Dias-Santagata D, Lifshits E, et al. Preexistence and clonal selection of MET amplification in EGFR mutant NSCLC. Cancer Cell 2010;17:77–88.

[10] Suda K, Murakami I, Katayama T, Tomizawa K, Osada H, Sekido Y, et al. Reciprocal and complementary role of MET amplification and EGFR T790M mutation in acquired resistance to kinase inhibitors in lung cancer. Clin Cancer Res 2010;16:5489–98.

[11] Kosaka T, Yatabe Y, Endoh H, Kuwano H, Takahashi T, Mitsudomi T. Mutations of the epidermal growth factor receptor gene in lung cancer: biological and clinical implications. Cancer Res 2004;64:8919–23.

[12] Onozato R, Kosaka T, Kuwano H, Sekido Y, Yatabe Y, Mitsudomi T. Activation of MET by gene amplification or by splice mutations deleting the juxtamembrane domain in primary resected lung cancers. J Thorac Oncol 2009;4: 5–11.

[13] Yao Z, Fenoglio S, Gao DC, Camiolo M, Stiles B, Lindsted T, et al. TGF-beta IL-6 axis mediates selective and adaptive mechanisms of resistance to molecular targeted therapy in lung cancer. Proc Natl Acad Sci USA 2010;107: 15535–40.

[14] Suda K, Tomizawa K, Fujii M, Murakami H, Osada H, Maehara Y, et al. Epithelial to mesenchymal transition in an epidermal growth factor receptor-mutant lung cancer cell line with acquired resistance to erlotinib. J Thorac Oncol 2011;6:1152–61.

[15] Chung JH, Rho JK, Xu X, Lee JS, Yoon HI, Lee CT, et al. Clinical and molecular evidences of epithelial to mesenchymal transition in acquired resistance to EGFR-TKIs. Lung Cancer 2011;73:176–82.

[16] Yamamoto C, Basaki Y, Kawahara A, Nakashima K, Kage M, Izumi H, et al. Loss of PTEN expression by blocking nuclear translocation of EGR1 in gefitinib-resistant lung cancer cells harboring epidermal growth factor receptor-activating mutations. Cancer Res 2010;70:8715–25.

[17] Serrano M, Lin AW, McCurrach ME, Beach D, Lowe SW. Oncogenic ras provokes premature cell senescence associated with accumulation of p53 and p16INK4a. Cell 1997;88:593–602.

[18] Giaccone G, Wang Y. Strategies for overcoming resistance to EGFR family tyrosine kinase inhibitors. Cancer Treat Rev 2011;37:456–64.

[19] Ercan D, Zejnullahu K, Yonesaka K, Xiao Y, Capelletti M, Rogers A, et al. Amplification of EGFR T790M causes resistance to an irreversible EGFR inhibitor. Oncogene 2010;29:2346–56.

[20] Sos ML, Koker M, Weir BA, Heynck S, Rabinovsky R, Zander T, et al. PTEN loss contributes to erlotinib resistance in EGFR-mutant lung cancer by activation of Akt and EGFR. Cancer Res 2009;69:3256–61.

[21] Collado M, Gil J, Efeyan A, Guerra C, Schuhmacher AJ, Barradas M, et al. Tumour biology: senescence in premalignant tumours. Nature 2005;436: 642.

[22] Boucher MJ, Jean D, Vezina A, Rivard N. Dual role of MEK/ERK signaling in senescence and transformation of intestinal epithelial cells. Am J Physiol 2004;286:G736–46.

[23] Riely GJ, Kris MG, Zhao B, Akhurst T, Milton DT, Moore E, et al. Prospective assessment of discontinuation and reinitiation of erlotinib or gefitinib in patients with acquired resistance to erlotinib or gefitinib followed by the addition of everolimus. Clin Cancer Res 2007;13:5150–5.

Activated Leukocyte Cell-Adhesion Molecule (ALCAM) Promotes Malignant Phenotypes of Malignant Mesothelioma

Futoshi Ishiguro, MD,*† Hideki Murakami, MD, PhD,* Tetsuya Mizuno, MD,*†
Makiko Fujii, DDS, PhD,* Yutaka Kondo, MD, PhD,* Noriyasu Usami, MD, PhD,†
Kohei Yokoi, MD, PhD,† Hirotaka Osada, MD, PhD,*‡ and Yoshitaka Sekido, MD, PhD*‡

Introduction: Cell-adhesion molecules play important roles involving the malignant phenotypes of human cancer cells. However, detailed characteristics of aberrant expression status of cell-adhesion molecules in malignant mesothelioma (MM) cells and their possible biological roles for MM malignancy remain poorly understood.

Methods: DNA microarray analysis was employed to identify aberrantly expressing genes using 20 MM cell lines. Activated leukocyte cell-adhesion molecule (ALCAM) expression in MM cell lines was analyzed with quantitative reverse transcription-polymerase chain reaction and Western blot analyses in 47 primary MM specimens with immunohistochemistry. ALCAM knockdown in MM cell lines was performed with lentivirus-mediated short hairpin RNA (shRNA) transduction. Purified soluble ALCAM (sALCAM) protein was used for in vitro experiments, whereas MM cell lines infected with the sAL-CAM-expressing lentivirus were tested for tumorigenicity in vivo.

Results: ALCAM, a member of the immunoglobulin superfamily, was detected as one of the most highly upregulated genes among 103 cell-adhesion molecules with microarray analysis. Elevated expression levels of ALCAM messenger RNA and protein were detected in all 20 cell lines. Positive staining of ALCAM was detected in 26 of 47 MM specimens (55%) with immunohistochemistry. ALCAM knockdown with shRNA suppressed cell migration and invasion of MM cell lines. Purified sALCAM protein impaired the migration and

invasion of MM cells in vitro, and the infection of sALCAM-expressing virus into MM cells significantly prolonged survival periods of MM-transplanted nude mice in vivo.

Conclusion: Our study suggests that overexpression of ALCAM contributes to tumor progression in MM and that ALCAM might be a potential therapeutic target of MM.

Key Words: Activated leukocyte cell-adhesion molecule (ALCAM), Malignant mesothelioma, Migration, Invasion, Soluble isoform.

Malignant mesothelioma (MM) is an aggressive tumor arising from mesothelial cells of the pleural or peritoneal cavity, and exposure to asbestos is considered to play a crucial role in tumor development.[1-5] Despite advances in the chemotherapeutical modalities combining cisplatin and antifolate agent such as pemetrexed[6] or the trials of radical multimodal therapy including neoadjuvant chemotherapy followed by extrapleural pneumonectomy and hemithoracic radiation,[7-9] the prognosis of patients with MM remains very poor. New approaches to the treatment are needed to improve their outcome.

Aberrant expressions of cell-adhesion molecules in cancer cells play important roles in cell proliferation, migration, and metastasis.[10,11] As for cell-adhesion molecules associated with MM, positivity of N-cadherin or CD141 and negativity of E-cadherin or CD15 have been proposed to be useful diagnostic findings for the epithelial type of MM.[12] Recently, CD146 has been proposed as an immunocytochemical marker for differential diagnosis of MM from reactive mesothelium.[13] However, only a few reports have aimed to resolve the relationship between aberrant expression of cell-adhesion molecules and MM progression.[14-16]

Activated leukocyte cell-adhesion molecule (ALCAM/CD166) is a type-I transmembrane protein and a member of the immunoglobulin superfamily.[17,18] ALCAM comprises five extracellular immunoglobulin-like molecules (D1–D5), a transmembrane domain, and a short COOH-terminal cytoplasmic tail (Supplementary Figure 1A, Supplemental Digital Content 1, http://links.lww.com/JTO/A259).[19] ALCAM was first identified on activated leukocytes as a ligand of CD6,[20,21] and ALCAM-CD6-mediated adhesion was shown to contribute

to T-cell activation or proliferation.[22,23] Meanwhile, ALCAM was also demonstrated to mediate homophilic ALCAM-to-ALCAM interaction,[24,25] which was shown to be involved in physiological processes including angiogenesis,[26] immune response,[27] and cell migration during the neuronal development.[28] As for carcinogenesis, ALCAM has been reported to participate in the promotion of cell migration or invasion in vitro[29,30] and the enhancement of tissue invasion and metastases in vivo.[31] In primary malignant tumors, overexpression of ALCAM has also been demonstrated to be pathologically correlated with aggressiveness in colorectal cancer,[32] gastric cancer,[33] and various types of cancers.[34–39]

Meanwhile, a soluble isoform of ALCAM (sALCAM) has also been identified as an alternative, shortened ALCAM transcript.[26] This transcript contains only one of the five immunoglobulin domains, D1, which was shown to be the most important region for ligand binding (Supplementary Figure 1C, Supplemental Digital Content 1, http://links.lww.com/JTO/A259).[25] sALCAM was shown to block homophilic binding of ALCAM, and was considered to have a regulatory role in blocking endogenous ALCAM function.[27] Moreover, sALCAM was also demonstrated to inhibit tumor progression; sALCAM treatment impaired melanoma cell migration in vitro and diminished metastatic properties in vivo.[31]

In this study, we found ALCAM to be one of the most upregulated genes among cell-adhesion molecule-encoding genes in MM cell lines and showed the overexpression of ALCAM in more than half of MM primary tumors. We showed that ALCAM knockdown by short hairpin RNA (shRNA) exerted inhibitory effects on cell migration and invasion of MM cells. Furthermore, we demonstrated that the sALCAM attenuated the malignant phenotypes of MM cells in vitro and that a xenographic murine model inoculated with MM cells that were infected with sALCAM-expressing lentivirus showed a prolonged survival. Our results indicate that ALCAM has a significant role in MM cell progression and that ALCAM may well be a molecular target against MM cells.

MATERIALS AND METHODS

Cell Lines and Primary Specimens of MM

Fourteen Japanese MM cell lines, including ACC-MESO-1, -4, Y-MESO-8D, -9, -12, -14, -21, -22, -25, -26B, -27, -28, -29, and -30, were established in our laboratory as reported previously and described elsewhere, and the cells at 10 to 15 passages were used for assays.[40] Four MM cell lines including NCI-H28, NCI-H2052, NCI-H2373, and MSTO-211H, and one immortalized mesothelial cell line, MeT-5A, were purchased from the American Type Culture Collection (ATCC) (Rockville, MD), and cells at 3 to 5 passages were used. NCI-H290 and NCI-H2452 were the kind gift of Dr. Adi F. Gazdar. All MM cell lines were cultured in RPMI1640 medium supplemented with 10% fetal calf serum and 1× antibiotic-antimycotic (Invitrogen, Carlsbad, CA) at 37°C in a humidified incubator with 5% CO_2. MeT-5A was cultured according to ATCC instructions. Two primary cultures of normal mesothelial cells at 3 to 5 passages derived from ascites of patients with ovarian cancer, OV-M1, gastric cancer, GAS-

M1, were also used. Forty-seven primary specimens of MMs used included 35 pleura, 6 peritoneum, and 6 other sites of origins. Histological classification was 34 epithelial, 6 biphasic, 5 spindle, 1 desmoplastic, and 1 lymphohistiocytoid. Among 47 MMs, 28 were MM tissue samples obtained from patients at Aichi Cancer Center Hospital, Nagoya University Hospital, Japanese Red Cross Nagoya First Hospital, Toyota Kosei Hospital, and Kasugai Municipal Hospital according to the Institutional Review Board-approved protocol of each and the written informed consent from each patient. Fifteen primary MM samples were obtained as result of biopsy, 11 samples via extrapleural pneumonectomy and 2 samples were collected via pleurectomy/decortication. Overall survival was measured from the date of surgery until death or the final date of the follow-up. The median length of follow-up for patients was 12 months (range, 2–38 months). Normal lung samples were obtained from patients with lung cancer who had undergone curative pulmonary resection. The other 19 MM samples were from the human mesothelioma tissue array from US Biomax (Rockville, MD).

Antibodies

Mouse anti-ALCAM antibody (clone MOG/07 and SNCL-CD166) for Western blot and immunohistochemical analysis was purchased from Novocastra (Newcastle, U.K.). Mouse anti-ALCAM (clone 3A6, 559260) for immunofluorescence was purchased from BD Bioscience Discovery Labware (Bedford, MA) and mouse anti-β-actin (clone AC74) was from Sigma (St. Louis, MO). Rabbit anti-β-catenin antibody (sc-7199) was purchased from Santa Cruz Biotechnology (Santa Cruz, CA), and mouse anti-V5 was from Invitrogen.

Construction of RNA Interference Vectors and Expression Vectors

Complementary short hairpin (sh) sequence was cloned into pLentiLox3.7[41] under control of a U6 promoter and transfected into HEK293FT cells along with the vectors of VSVG, RSV-Rev, and pMDLg-pRPE, to generate lentiviruses that transcribe shRNA. Two sh oligonucleotides were designed for two different sequences within the ALCAM open reading frame (ALCAM-Sh1, 5′-GAGGAATCTCCTTATATTA-3′ and ALCAM-Sh2, 5′-GGATAACATCACTCTTAAA-3′). Control vectors, ALCAM-Scr1 (5′-GTTTACCACGGAATATTAT-3′) and ALCAM-Scr2 (5′-GAAACCTTTTCAGCAATAA-3′) were constructed using oligonucleotides with scrambled sequence for ALCAM-Sh1 and ALCAM-Sh2. The efficacy of each virus was tested by immunoblotting of whole cell lysates 96 hours after infecting NCI-H290 cells at the multiplicity of infection of 10. The cDNA fragments of wild-type ALCAM or sALCAM were amplified by PCR using PrimeSTAR Max DNA polymerase (Takara Bio, Otsu, Japan), and introduced into the pcDNA3.1 V5-His expression vector (Invitrogen), thereby fusing these cDNAs with the V5-His sequence. The sequences of all constructs were confirmed. To generate wild-type ALCAM- or sALCAM-expressing lentiviral vectors, cDNA coding for ALCAM or sALCAM tagged with V5-His was amplified with PCR and cloned into the pLL3.7Lox

lentiviral vector with an infusion cloning system (Clontech, Mountain View, CA).

Purification of sALCAM

HEK293FT cells were infected with V5-His-tagged sALCAM-expressing or empty virus as a control. Ninety-six hours after infection, the media were exchanged to serum-free medium and cells were incubated for 24 hours. The conditioned media were collected and subjected to purification of sALCAM using the His-tagged protein purification kit (Qiagen K.K., Tokyo, Japan). Purified His-tagged proteins were dialysed to remove buffer-containing imidazole and sodium using Biotech Cellulose Ester membranes (Spectrum Laboratories, Rancho Dominguez, CA). Then, proteins were filtrated at a concentration of 20-fold using Amicon Ultra-0.5 devices (Millipore, Bedford, MA).

Animals and Implantation Model

Female KSN/Slc nude mice (nu/nu) were obtained from Japan SLC (Hamamatsu, Japan) and maintained under specific pathogen-free conditions throughout this study. NCI-H290 cells either infected with sALCAM-V5- or GFP-lentivirus were harvested using trypsin/EDTA, washed twice, and suspended in phosphate-buffered saline. Six-week-old mice were injected with 1×10^6 cells in 100 μl of PBS into the right thoracic cavity. Survival was measured from the date of injection of MM cells until death. All experiments were performed in accordance with the guidelines established by the Aichi Cancer Center Committee on Animal Care and Use.

Additional materials and methods are described in Supplementary Material and Methods (Supplemental Digital Content 2, http://links.lww.com/JTO/A260).

RESULTS

ALCAM Expression in MM Cell Lines and Primary Tissues

To determine what types of cell-adhesion molecules are aberrantly expressed in MM cells, we performed microarray analysis using 20 MM cell lines. Among 103 genes that encode cell-adhesion molecules from the array, we listed the top 10 genes that showed either up- or downregulation in MM cells (Supplementary Table 1, Supplemental Digital Content 3, http://links.lww.com/JTO/A261). Because ALCAM was the second- highest scoring gene and has been reported to be associated with other types of human malignancies, we focused on ALCAM for its roles in the pathogenesis of MM. To validate the microarray data, we next examined the expression status of ALCAM with quantitative reverse transcription-polymerase chain reaction and Western blot analyses. Comparing with the expression level of ALCAM mRNA in an immortalized mesothelial cell line, MeT-5A, which was arbitrarily set as 1.0, all 20 cell lines expressed more than 4.5-fold ALCAM mRNA, with 15 cell lines being more than 20-fold (Fig. 1A). Meanwhile, two primary cell cultures of normal mesothelial cells, OV-M1, and GAS-M1, also showed relatively low expression of ALCAM. Western blot analysis also confirmed increased ALCAM protein in all 20 cell lines, which seemed

to be consistent with mRNA expression levels (Fig. 1B). Each MM cell line expressed ALCAM of different sizes. The different sizes of ALCAM were thought to be not only because of different posttranslational modifications of the ALCAM protein such as glycosylation, but also because of splice variants (variant 1, 2, and 3) of the *ALCAM* gene, with the estimated molecular weight of each being 65.1, 63.6, and 61.9 kDa, respectively.[19] We also performed immunocytochemical analysis using NCI-H290 cells and observed strong signals at cell-to-cell interaction regions (Fig. 1C). However, ALCAM signals in MeT-5A cells were undetectable (Fig. 1C).

To study whether ALCAM expression detected in MM cell lines reflects primary MMs, we investigated ALCAM expression in 47 MM specimens with immunohistochemical analysis. We detected 9 specimens (19%) for 3+, 17 (36%) for 2+, 14 (30%) for 1+, and 7 (15%) for 0 score, indicating that 26 of 47 specimens (55%) were positive (3+ or 2+) for ALCAM. As five specimens were the origins of cell lines, we compared them and found that four pairs of cell lines and primary tumors (Y-MESO-9/KD1048, Y-MESO-12/KD1050, Y-MESO-14/KD1053, and Y-MESO-21/KD1056) showed a well-concordant expression of ALCAM (Figs. 2A–D). Although the Y-MESO-26B cell line showed a high expression of ALCAM, its corresponding primary specimen, KD1062, showed faint staining (1+) of ALCAM (Fig. 2E). Meanwhile, normal pleural mesothelial cells also showed faint staining (1+) (Fig. 2F). We investigated the relationship between the ALCAM immunohistochemical staining status and clinicopathological characteristics of MMs. However, there was no significant relationship between ALCAM expression and the sites of origin or histological subtypes (Supplementary Table 2, Supplemental Digital Content 4, http://links.lww.com/JTO/A262). Survival data of 22 patients were also available from 28 of our patients. However, we did not detect a significant association between the ALCAM expression and the patients' survival (data not shown).

Inhibition of ALCAM-Suppressed Migration and Invasion of Mesothelioma Cells

As ALCAM is reportedly involved in the promotion of tumor cell migration and invasion in other types of human malignancies, we investigated whether or not inhibition of ALCAM suppresses malignant phenotypes of MM cells. We selected H290 and Y-MESO-27 as representative cell lines with high and moderate ALCAM protein expression, respectively. We synthesized two ALCAM shRNA constructs and confirmed ALCAM-Sh1 suppressed ALCAM protein expression more efficiently than ALCAM-Sh2 in two mesothelioma cell lines (Fig. 3A). Using these ALCAM-Sh constructs, we found that ALCAM knockdown induced 30 to 50% inhibition of cell migration and invasion of both cell lines (Fig. 3B). We further carried out colony formation assay and found that ALCAM knockdown also impaired anchorage-independent cell growth (Fig. 3C). However, we did not detect the inhibitory effect on cell proliferation by ALCAM knockdown (Supplementary Figure 2, Supplemental Digital Content 5, http://links.lww.com/JTO/A263).
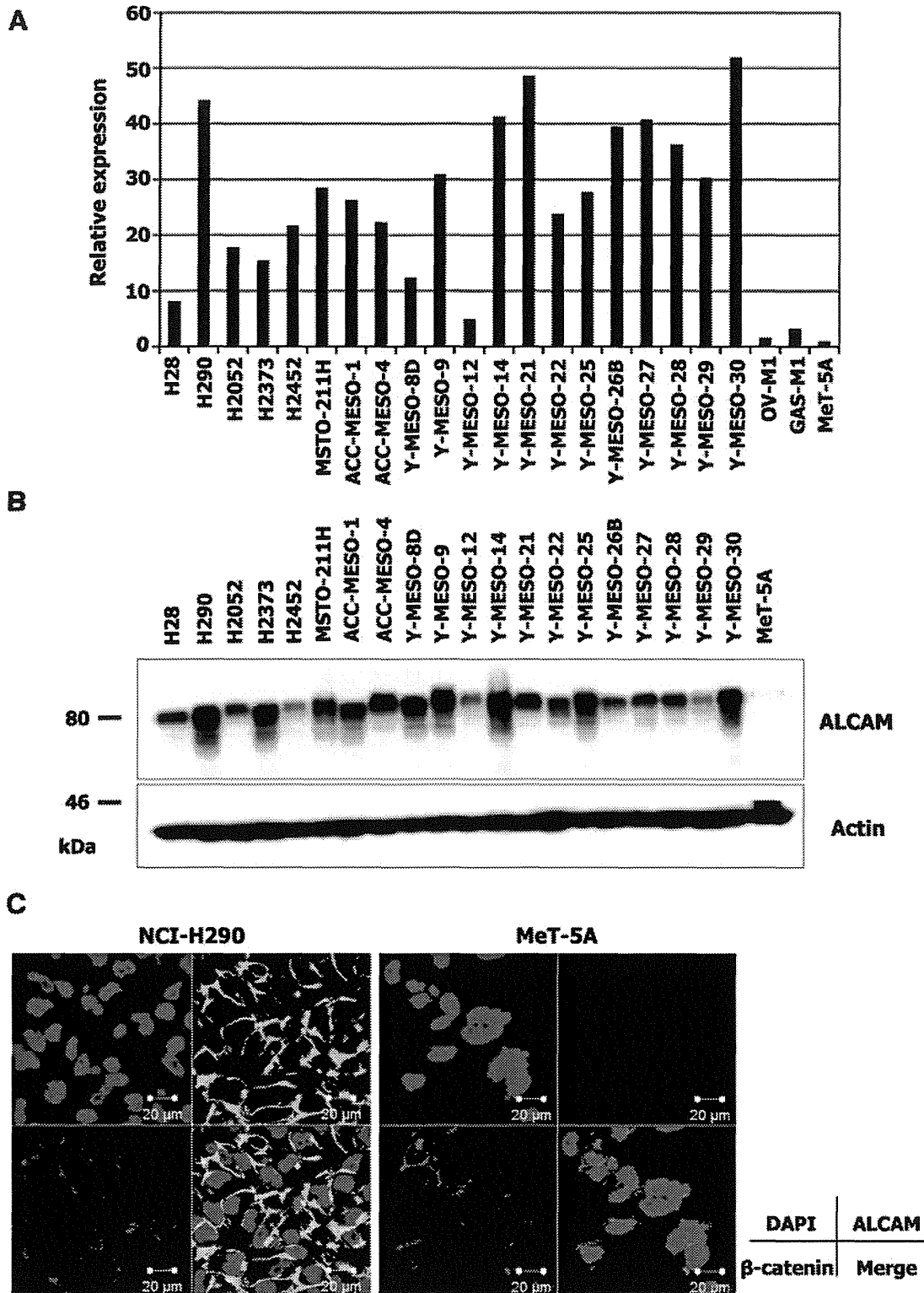
FIGURE 1. Expression of ALCAM in MM cell lines. (*A*) Quantitative RT-PCR analysis of ALCAM in 20 MM cell lines, 1 immortal-ized cell line, MeT-5A, and 2 primary normal mesothelial cultures, OV-M1 and GAS-M1. Relative expression of MeT-5A was arbitrarily set at 1.0, (*B*) Western blot analysis of ALCAM in 20 MM cell lines. Expression of β-actin was used as the control, (*C*) Immunocytochemical analysis. Strong, membranous signals of ALCAM were observed in NCI-H290 cells, but no signals in MeT-5A cells. β-catenin staining was used as the marker of the cell-to-cell interaction region. ALCAM, Activated leukocyte cell-adhesion molecule; MM, malignant mesothelioma; RT-PCR, reverse transcription polymerase chain reaction.
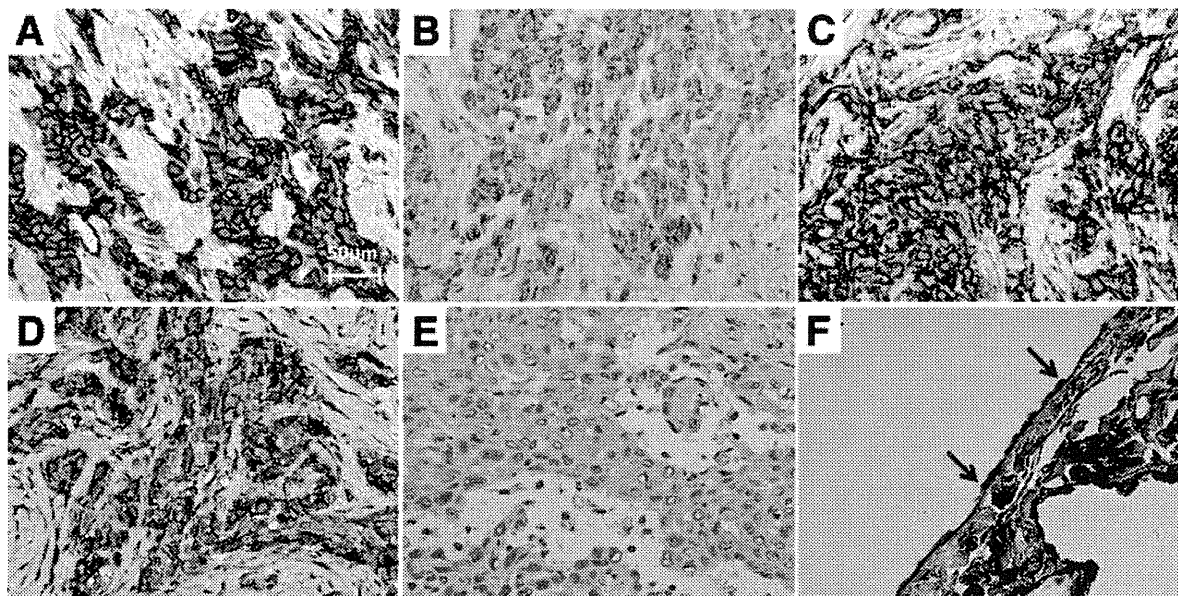
FIGURE 2. Immunohistochemical analysis of ALCAM in primary MM specimens. ALCAM was positive in KD1048 (3+) (*A*), KD1050 (2+) (*B*), KD1053 (3+) (*C*), and KD1056 (3+) (*D*). These samples were the origins of Y-MESO-9 cell line (20.2 for relative ALCAM mRNA level), Y-MESO-12 (4.7), Y-MESO-14 (35.2), and Y-MESO-21 (51.6), respectively, as shown in Figure 1*A*. Although KD1062 showed faint staining (1+) (*E*), its corresponding cell line, Y-MESO-26B, showed high ALCAM expression (30.4). Normal pleural mesothelial cells (arrows) (*F*) showed faint staining (1+) of ALCAM. ALCAM, Activated leukocyte cell-adhesion molecule; MM, malignant mesothelioma; mRNA, messengerRNA.

ALCAM Induces Enhancement of Migration and Anchorage-Independent Growth of Normal Mesothelial Cells

To determine whether ALCAM confers malignant phenotypes to normal mesothelial cells, we infected the wild-type ALCAM virus into MeT-5A cells (Fig. 4*A*). With immunocytochemical analysis, we confirmed that ectopically expressed ALCAM was localized at the cell-to-cell interaction regions (Fig. 4*B*). We found that the transduction of ALCAM increased cell migration and anchorage-independent cell growth of MeT-5A cells (Fig. 4*C*). However, we could not observe the enhancement of cell invasion ability (data not shown). As expected, we did not detect promotion of MeT-5A cell proliferation with enhanced ALCAM expression (Supplementary Figure 3, Supplemental Digital Content 6, http://links.lww.com/JTO/A264); this suggested that ALCAM does not affect cell proliferation itself as seen in ALCAM-knockdown MM cells.

Regulatory Effect of sALCAM on ALCAM Function

To evaluate a possible inhibitory effect of the soluble form, sALCAM (Supplementary Figure 1C, Supplemental Digital Content 1, http://links.lww.com/JTO/A259), on MM cells we generated sALCAM expression virus with V5-epitope tag that was attached at the COOH-terminal, and infected HEK293FT cells with them to synthesize sALCAM protein. With Western blot analysis using anti-V5 antibody, sALCAM was detected in the cell lysates and conditioned culture medium of HEK293FT/sALCAM-V5 cells (Fig. 5*A*). We then purified the His-tagged sALCAM protein from conditioned

culture medium, and the purity was confirmed by silver staining (Fig. 5*B*). We added sALCAM in the culture medium of MM cell lines and found that sALCAM induced 20 to 40% inhibition of cell migration and invasion of MM cells (Fig. 5*C*). We further demonstrated that purified sALCAM significantly impaired anchorage-independent cell growth of MM cells (Fig. 5*D*). However, we did not observe any inhibitory effect of sALCAM on cell proliferation (Supplementary Figure 5, Supplemental Digital Content 1, http://links.lww.com/JTO/A265).

Survival Benefit of sALCAM in MM Cell-Bearing Nude Mice

To assess the possible therapeutic effect of sALCAM in vivo, we infected NCI-H290 cells with sALCAM-expressing virus and injected them into the right thoracic cavity of nude mice. We found that nude mice inoculated with the MM cell line with sALCAM expression, NCI-H290/sALCAM-V5, exhibited significantly prolonged survival time, compared with the control, NCI-H290/GFP (Fig. 6). Autopsy using Western blot and immunohistochemical analyses served to confirm stable expression of sALCAM in the thoracic tumors (Supplementary Figure 5, Supplemental Digital Content 8, http://links.lww.com/JTO/A266).

DISCUSSION

In the present study, we found that ALCAM is one of the most highly upregulated genes among cell adhesion-related genes in MM cells and that ALCAM gives a malignant phenotype to MM cells. We showed elevated expression of
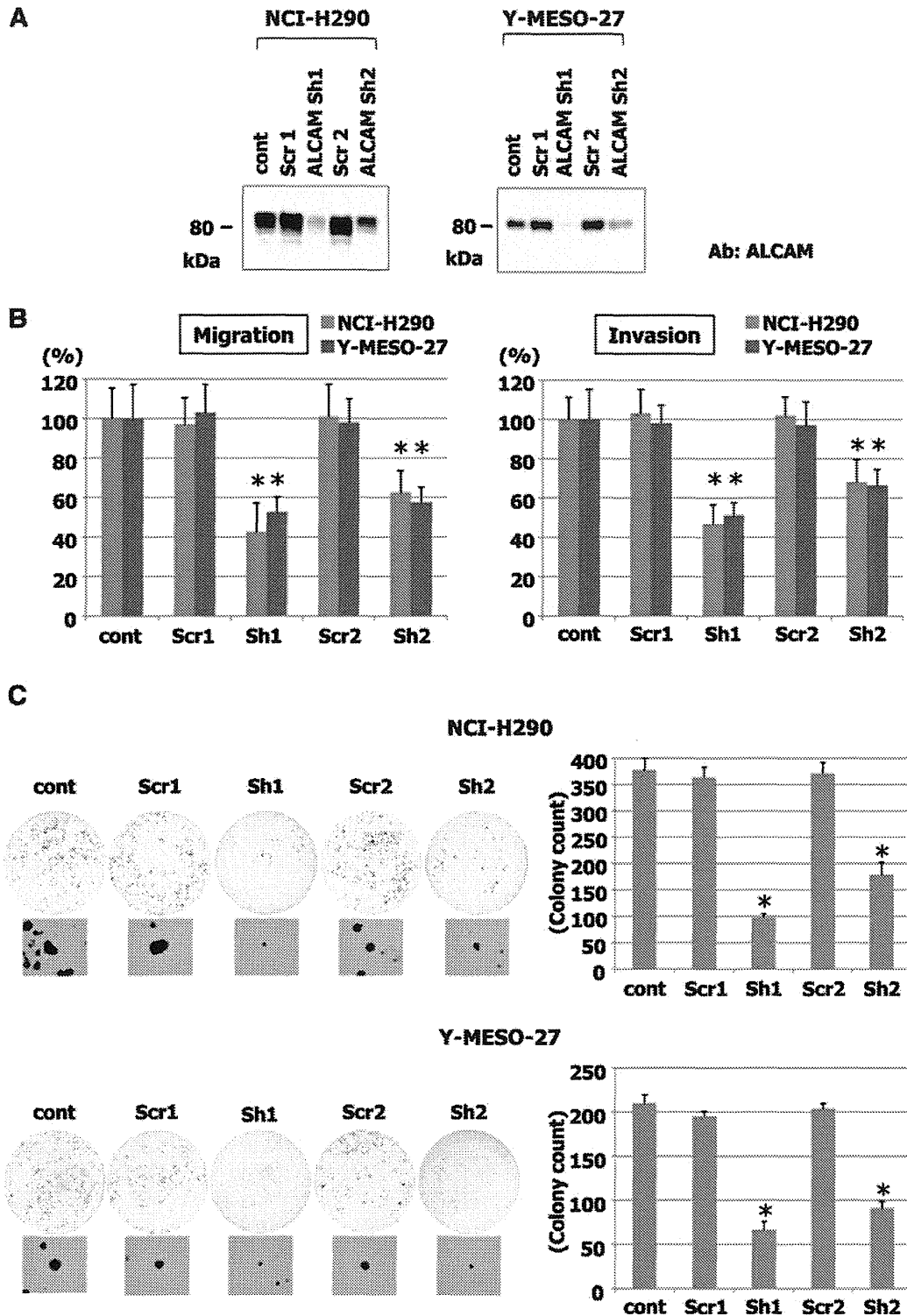
FIGURE 3. Lentiviral shRNA-mediated ALCAM knockdown in two MM cell lines, NCI-H290 and Y-MESO-27. (*A*) Western blot analysis demonstrates efficiency of ALCAM knockdown. Both ALCAM-Sh vectors, ALCAM Sh1 and ALCAM Sh2, showed effective suppression of the level of ALCAM protein, whereas the control vectors, ALCAM Scr1 and ALCAM Scr2, showed no inhibition. Cells were lysed 96 hours after infection. (*B*) ALCAM knockdown inhibited migration and invasion of two MM cell lines. (*C*) Inhibition of ALCAM with shRNA-mediated knockdown in MM cell lines suppressed anchorage-independent colony formation. Representative results of the NCI-H290 and Y-MESO-27 cell lines are shown (top) with higher magnifications of their representative colonies (bottom). The results of the triplicate experiments are presented. Columns, mean; bars, SD. ALCAM, Activated leukocyte cell-adhesion molecule; MM, malignant mesothelioma; shRNA, short hairpin RNA. *$p < 0.05$ vs. control.
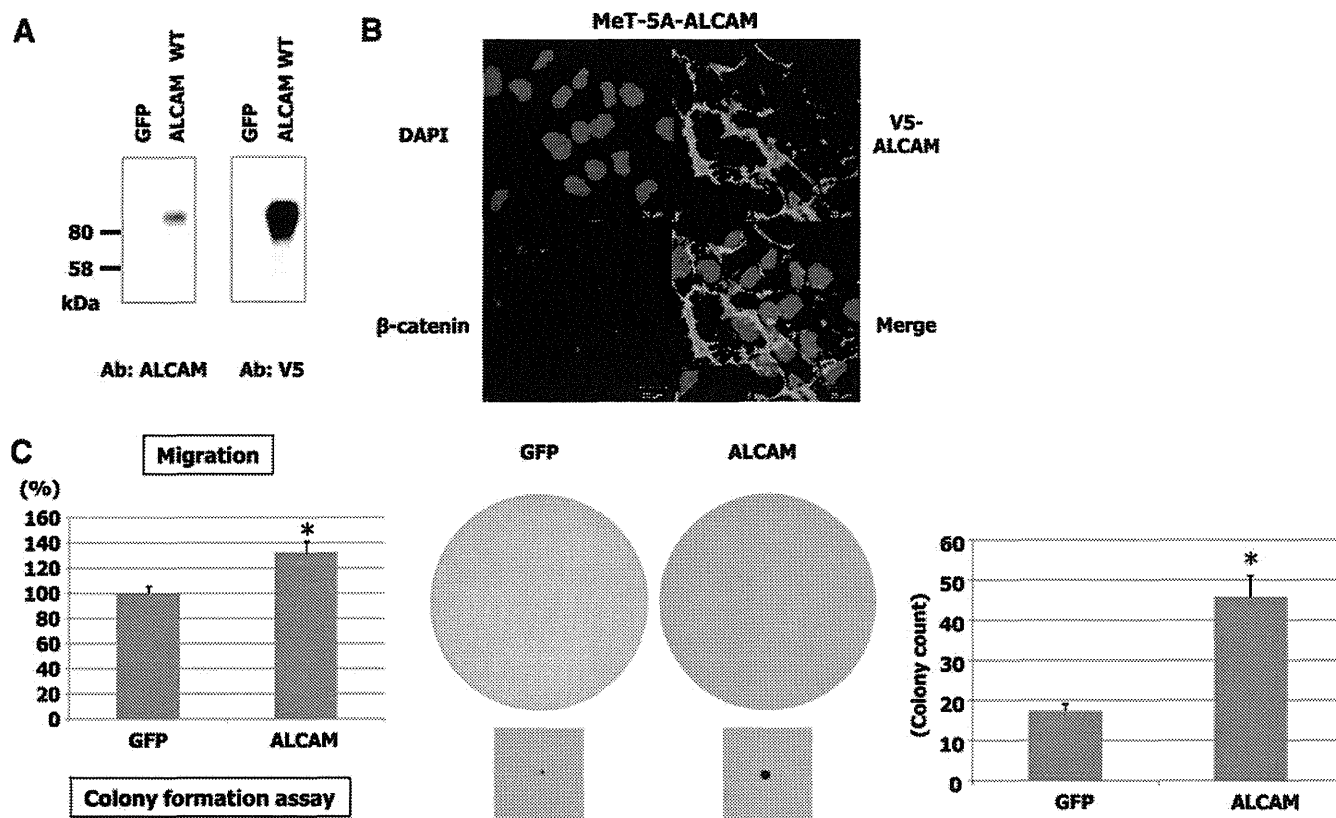
FIGURE 4. Enhancement of cell migration and anchorage-independent growth of immortalized mesothelial cells, MeT-5A, with infection of ALCAM expressing virus. (*A*) Western blot analysis. Whole cell lysates of MeT-5A cells were obtained 96 hours after infection of wild-type ALCAM or green fluorescent protein virus. (*B*) Immunocytochemical analysis. Positive signals of ALCAM were detected mainly at the cell-cell junction. (*C*) Cell migration and colony formation analysis of MeT-5A cells. Exogenous ALCAM enhanced migration and anchorage-independent cell growth of the MeT-5A cells. Columns, mean; bars, SD. ALCAM, Activated leukocyte cell-adhesion molecule; MM, malignant mesothelioma. *$p < 0.05$ versus GFP control.

ALCAM in most MM cell lines and 55% surgical specimens of MMs. ALCAM's oncogenic properties served to promote migration and invasion in MM cells. Moreover, we demonstrated that the soluble isoform, sALCAM, impaired migration and invasion of MM cells in vitro and that sALCAM-expressing virus infection prolonged the survival of MM cell-transplanted mice.

Elevated ALCAM expression was previously reported in melanoma and breast cancer cell lines,[30,42] and immunohistochemical analysis of primary tumors revealed ALCAM expression in 36 to 57% of melanoma, pancreatic cancer, and bladder cancer.[29,34,36] Thus, the frequency of elevated ALCAM expression in MM tumors seemed to be similar to or higher than that of other types of human malignancies. As for the possible mechanisms of ALCAM overexpression, our comparative genomic hybridization analysis did not detect gene amplification of 3q13 locus,[43] which is the locus of the *ALCAM* gene. Meanwhile, a recent report by King et al[42] indicated that nuclear factor kappa B (NF-κB) binds to a consensus-binding motif in the human *ALCAM* promoter and enhances its promoter activity. In this regard, because NF-κB was also shown to be induced in asbestos-exposed mesothelial cells and to play a critical role in the promotion

and progression of MM cells,[44,45] NF-κB might be one of the underlying mechanisms of the ALCAM upregulation in MM cells.

We demonstrated that ALCAM promotes cell migration and invasion, but not cell proliferation, in MM cells. There are several possible mechanisms that the homophilic ALCAM cell-to-cell adhesion confers malignant phenotypes to cells. For instance, ALCAM cell adhesion was shown to contribute to the activation of matrix metalloproteinase-2 (MMP-2), which is involved in tissue invasion, metastases, and angiogenesis.[30,31] It was also indicated that short interfering RNA-mediated ALCAM knockdown inhibited activation of MMP-2 in melanoma and fibrosarcoma cells.[30] Thus, these results suggested that the role of ALCAM might be to initiate a signal to trigger MMP-2 activation. However, we did not confirm a clear MMP-2 inactivation in MM cells infected with the ALCAM-Sh1 expressing virus (data not shown). In addition, although we further performed phospho-kinase and phospho-receptor thyrosin kinase arrays to explore possible cellular mechanisms revealing how ALCAM confers malignant phenotypes to MM cells, our knockdown experiments did not detect significant changes in phosphorylation status of all 88 proteins (data not shown).
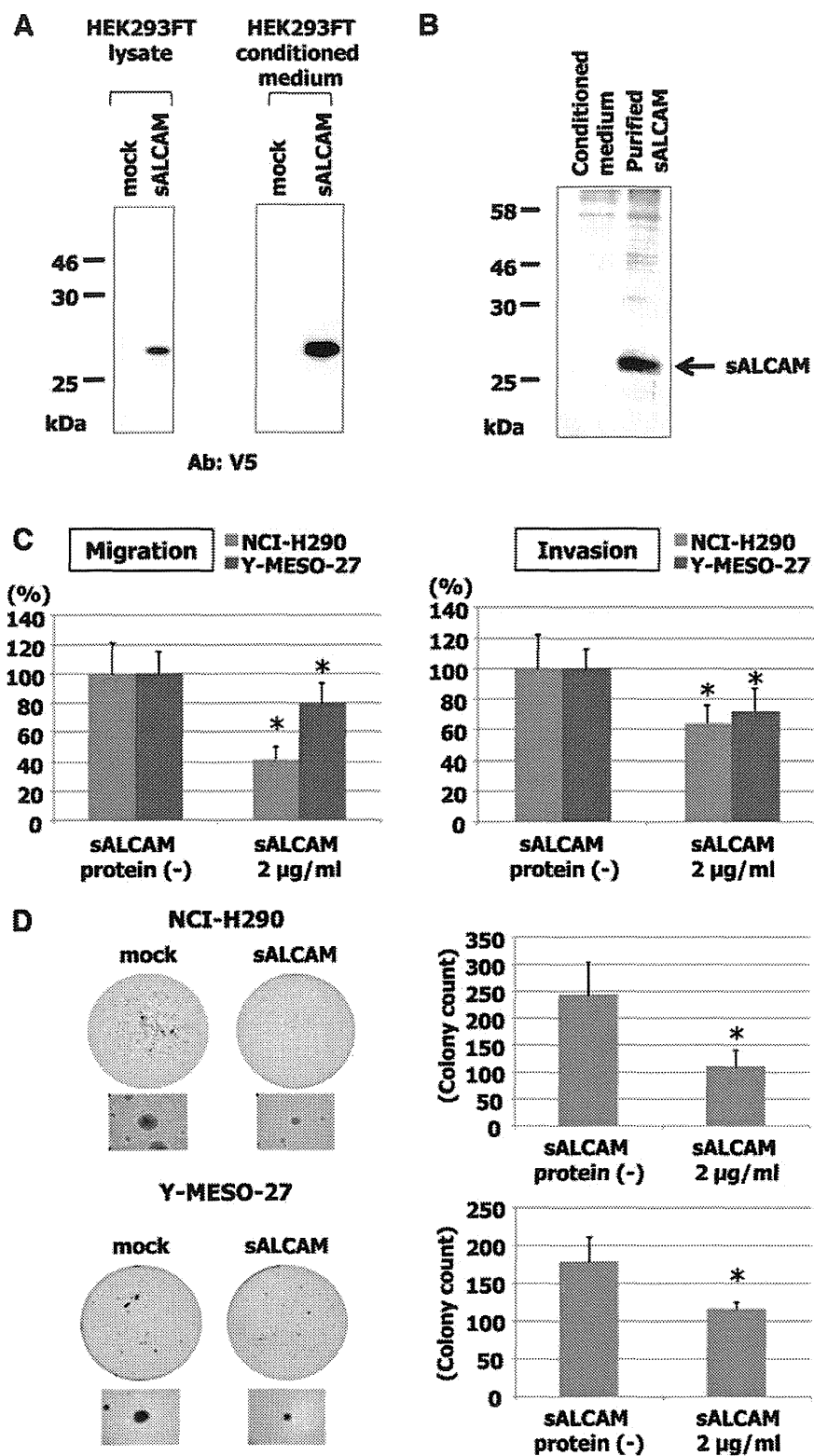
FIGURE 5. Purification of sALCAM and its inhibitory effects on MM cells. (A) Western blot analysis using anti-V5 antibody. Secreted sALCAM in the conditioned medium as well as in the whole cell lysates was confirmed. (B) Silver staining. Purity of synthesized sALCAM was confirmed with no obvious contaminated proteins. (C) Cell migration and invasion assays. In the presence of sALCAM protein at the indicated final concentration in the media, both migration and invasion abilities of MM cells were significantly inhibited. (D) Anchorage-independent colony formation assay. Anchorage-independent growth of NCI-H290 and Y-MESO-27 cell lines was suppressed with addition of sALCAM. Columns, mean; bars, SD. sALCAM, soluble activated leukocyte cell-adhesion molecule; MM, malignant mesothelioma. *$p < 0.05$ vs. control.

The extracellular domain of adhesion molecules can be released from cells to yield soluble cell-adhesion molecules, which are generated by proteolytic cleavage or alternative splicing.[46–48] Regulatory roles of several soluble cell adhesion molecules have been shown to be involved in angiogenesis or tumor growth for intercellular adhesion molecule-1 [49,50] and in cell migration for P-selectin.[51] As for the soluble form sAL-CAM, Kilsdonk et al[31] showed that overexpressed sALCAM